symmetry

MDPI

Review

Magnetohydrodynamic Waves in Asymmetric Waveguides and Their Applications in Solar Physics—A Review

Robertus Erdélyi [1,2,3,*] and Noémi Kinga Zsámberger [1,4,5]

[1] Solar Physics and Space Plasma Research Centre, School of Mathematics and Statistics, University of Sheffield, Hicks Building, Hounsfield Road, Sheffield S3 7RH, UK
[2] Department of Astronomy, Eötvös Loránd University, 1/A Pázmány Péter Sétány, H-1117 Budapest, Hungary
[3] Gyula Bay Zoltán Solar Observatory (GSO), Hungarian Solar Physics Foundation (HSPF), Petőfi Tér 3, H-5700 Gyula, Hungary
[4] Department of Physics, University of Debrecen, Egyetem Tér 1, H-4010 Debrecen, Hungary
[5] Doctoral School of Physics, University of Debrecen, Egyetem Tér 1, H-4010 Debrecen, Hungary
* Correspondence: robertus@sheffield.ac.uk

Abstract: The solar atmosphere is a complex, coupled, highly dynamic plasma environment, which shows rich structuring due to the presence of gravitational and magnetic fields. Several features of the Sun's atmosphere can serve as guiding media for magnetohydrodynamic (MHD) waves. At the same time, these waveguides may contain flows of various magnitudes, which can then destabilise the waveguides themselves. MHD waves were found to be ubiquitously present in the solar atmosphere, thanks to the continuous improvement in the spatial, temporal, and spectral resolution of both space-born and ground-based observatories. These detections, coupled with recent theoretical advancements, have been used to obtain diagnostic information about the solar plasma and the magnetic fields that permeate it, by applying the powerful concept of solar magneto-seismology (SMS). The inclusion of asymmetric shear flows in the MHD waveguide models used may considerably affect the seismological results obtained. Further, they also influence the threshold for the onset of the Kelvin–Helmholtz instability, which, at high enough relative flow speeds, can lead to energy dissipation and contribute to the heating of the solar atmosphere—one of the long-standing and most intensely studied questions in solar physics.

Keywords: the Sun; solar magnetic fields; solar atmosphere; solar oscillations; solar coronal seismology; solar coronal waves

Citation: Erdélyi, R.; Zsámberger, N.K. Magnetohydrodynamic Waves in Asymmetric Waveguides and Their Applications in Solar Physics—A Review. *Symmetry* **2024**, *16*, 1228. https://doi.org/10.3390/sym16091228

Academic Editor: Toshio Tagawa

Received: 27 February 2024
Revised: 21 June 2024
Accepted: 3 July 2024
Published: 18 September 2024

1. Introduction

The past century, but especially the last few decades have seen solar telescope technology improve in leaps and bounds, including both Earth-based and space-borne instruments. Large telescopes on the ground, such as the Swedish Solar Telescope, La Palma (SST), Dunn Solar Telescope, Sac Peak (DST), New Vacuum Solar Telescope, Yunnan (NVST), Daniel K. Inouye Solar Telescope, Hawaii [1] (DKIST), as well as observing satellites like the Solar and Heliospheric Observatory (SoHO), Transition Region and Coronal Explorer (TRACE), Solar Dynamics Observatory (SDO), Interface Region Imaging Spectrograph (IRIS), Parker Solar Probe (PSP), or Solar Orbiter (SolO), to name a few of these excellent facilities, have made it possible to detect waves and oscillations at multiple wavelengths in the richly structured, magnetically coupled, dynamic environment of the solar atmosphere. In the near future, the next generation of large ground-based telescopes, such as the upgrade of DKIST and the European Solar Telescope (EST) Quintero Noda et al. [2], will push the boundaries of what we can observe even further, with a particular focus on the lower solar atmosphere; for some reviews in the context, see, e.g., [3,4], Banerjee et al. [5], Nakariakov et al. [6], and Jess et al. [7].

These high-resolution observations, combined with theoretical modelling, are invaluable tools to improve our understanding of magnetohydrodynamic (MHD) waves, which is a key factor in learning about the solar plasma itself. This is due to the ubiquitous presence of magnetic fields in our Sun's atmosphere, whose fine structures can then act as natural waveguides for propagating MHD waves. The motivation for studying solar MHD waves is at least two-fold: they can serve as mechanisms to transfer non-thermal energy between different layers and regions of the solar atmosphere, and they can also be utilised for the purposes of plasma diagnostics by solar magneto-seismology (SMS). Adding to the foundations of using oscillation measurements to study the internal structure of the Sun with helio-seismology (Leighton et al. [8], Ulrich [9], and Leibacher and Stein [10]), simple models were soon constructed to utilise wave information for investigating solar atmospheric structures as well (see an early review by Roberts et al. [11], early applications for magnetic field measurements by Nakariakov and Ofman [12], Wang et al. [13], and Erdélyi and Taroyan [14] for the exploration of density stratification in the corona by Andries et al. [15], and for measuring the adiabatic index by Van Doorsselaere et al. [16]). Among others, Nakariakov and Verwichte [17] and De Moortel and Nakariakov [18] provided reviews of identified MHD wave modes and seismological results in the corona. Advanced seismological techniques applicable to loop oscillations were also developed based on the frequencies of detected overtones (Andries et al. [19]) and the damping of oscillations (Ruderman and Erdélyi [20]). The overwhelmingly temporal-information-based methods of SMS were further complemented by spatial seismology studies, such as Guo et al. [21] and Chen et al. [22]. Again, this list only provides a brief glimpse into some milestones in the development of SMS and illustrative examples of each, as the literature has grown vastly in the past few years.

The field of SMS can only progress if advanced observations and theoretical studies go hand in hand, driving one another further forward, testing and validating theories, and interpreting surprising new observational results. The asymmetric environment of solar waveguides is a recent direction that a varied group of theoretical studies have pursued. The reason for this is that the asymmetry in the models can serve as a proxy for local inhomogeneity in, e.g., the magnetic field, the density, the temperature, and the bulk speed of flows present in the plasma. Incorporating the latter aspect into previously static models allows us to capture another essential aspect of the solar atmosphere: the widespread influence of plasma flows. For example, the concentration of the magnetic flux in the chromosphere creates a multitude of small plasma jets known as spicules (Beckers [23] and Sterling [24]), whose production and life-cycle rely on photospheric motions and shock waves (see De Pontieu et al. [25], Pereira et al. [26], and Martínez-Sykora et al. [27]). In turn, the spicules themselves can also serve as waveguides for MHD waves and as methods for energy transport to the higher solar atmosphere (Zaqarashvili and Erdélyi [28] and Komm et al. [29]) all around the solar disk. Furthermore, the presence of flows of various magnitudes and profiles also affects the properties of the waves guided by solar structures, and they can result in the appearance of instabilities, which, in turn, can lead to the destruction of the original waveguide. Studies focusing on asymmetric waveguides have prioritised the investigation of the Kelvin–Helmholtz instability (KHI), which can be observed, e.g., in prominences (Berger et al. [30], Ryutova et al. [31]). Other types of instabilities can also arise in the solar atmosphere and the Earth's magnetosphere due to the inhomogeneous distribution of plasma parameters (such as density, magnetic field strength, or flow speed gradients) in parts of the waveguide (see, e.g., Skirvin et al. [32], Yu et al. [33], Chen et al. [34], and Shi et al. [35]). Notable examples are the resonant flow instability, which may occur due to the presence of an Alfvén speed gradient and a velocity shear (Tirry et al. [36], Walker [37], and Taroyan and Erdélyi [38]); the double-gradient instability arising from the presence of gradients in the tangential and normal magnetic field components, leading to the appearance of so-called flapping waves in Earth's magnetotail current sheet (Erkaev et al. [39], Korovinskiy et al. [40], Zelenyi et al. [41]); and the dynamic kink instability (Zaqarashvili et al. [42]).

The aim of this review is to provide a summary of recent advances in the study of asymmetric solar waveguides, providing both a demonstration of the methods needed to derive analytical expressions that describe the dispersion of MHD waves in a given model, as well as a breakdown of the various sources of asymmetry that can and have been considered in these models, along with their specific effects on the properties of the waves supported by a given solar atmospheric structure. To achieve this, first, in Section 2, we give a more detailed introduction to the area of modelling MHD wave propagation in the solar atmosphere, especially with the purpose of carrying out SMS investigations. Then, in Section 3, we demonstrate how the currently most generalised multi-layered Cartesian waveguide model is constructed and how the dispersion relation is obtained for this most universal case. Next, we return to single-slab models and provide an overview of the specific effects of each additional source of waveguide asymmetry introduced into the system, gradually expanding the models to include first density, then magnetic, and eventually, flow asymmetry. In Section 4, a list of proposed applications of asymmetric slab models follows the general theoretical conclusions. Finally, we conclude the paper with an emphasis on key findings regarding the role of symmetry in the propagation of solar MHD waves and outline possibilities for further directions in which asymmetric models of solar structures may evolve in the future.

2. Methods: A Brief Account of MHD Wave Theory in Cartesian and Cylindrical Models

2.1. Solar Magneto-Seismology

The dynamic plasma environment of the solar atmosphere shows complex structuring, which follows the inhomogeneous distribution of ubiquitous magnetic fields. These, in turn, determine the distribution of plasma and generate a rich variety of solar waveguides. In studying these structures themselves, as well as the waves supported by them, the methods of solar magneto-seismology (SMS) provide a versatile and constantly evolving toolkit. The concept of SMS relies on the fact that the physical parameters and geometric structuring of a medium together determine the properties of the waves propagating through it. Some parameters of solar waveguide media may be determined from direct observations, such as temperature or density, as well as the geometric size of the structure. Furthermore, thanks to the increasing number and evolving technology of space-born and ground-based solar observatories, we can also measure temporal and spatial wave properties (periods and amplitudes) in a growing selection of solar phenomena. In addition, this is often more easily accomplished than a direct measurement of, e.g., transport coefficients or magnetic field strength.

On the other hand, from theoretical investigations, we can obtain a mathematical relationship between these (or other) "missing" parameters and the more easily measurable quantities. By combining the theoretical models with wave identifications from solar observations, and solving (often quite difficult) inversion problems, SMS studies provide estimates of the above-mentioned "missing" parameters of the solar atmospheric plasma. The first studies in this direction relying on direct visual observations of coronal loop oscillations were carried out by Aschwanden et al. [43] and Nakariakov et al. [44]. For reviews delving deeper into modelling efforts to this end and their relevance, see, e.g., Roberts et al. [11], Banerjee et al. [5], Andries et al. [19], Van Doorsselaere et al. [45], and Allcock et al. [46]. In the following, we provide a brief overview of the main directions and results of the analytical modelling efforts that SMS studies are built on. Building and understanding these theoretical models constitutes half of the methods of SMS, and it can be thought of as a common core of the field to return to when observations need to be evaluated.

2.2. On Flux Tube and Slab Models of the Solar Atmosphere

There are two popular fundamental geometric building blocks in theoretical MHD studies aiming to model solar atmospheric waveguides to carry out SMS investigations: the magnetic slab and the cylindrical flux tube waveguides. Both of these have different

applications in solar physics and provide theoretical opportunities to focus on different aspects of wave physics in our Sun's atmosphere.

2.2.1. Cartesian Models

The model family employing Cartesian geometry is often used to describe interfaces and slab-like structures in the solar atmosphere and the Earth's magnetosphere. The properties of magneto-acoustic waves guided by the "classical", symmetric slab models delineated by tangential discontinuities were explored in detail and the results summarised by Roberts [47,48], and Edwin and Roberts [49] in a series of seminal studies.

As the first step in this series, Roberts [47] investigated the propagation of magneto-acoustic surface waves at a single magnetic interface. Next, adding a new layer of complexity to the problem, Roberts [48] considered two interfaces separating an internal slab of magnetised plasma from a symmetric, non-magnetic environment, thus constructing the simplest model of a three-layer symmetric magnetic slab waveguide system. Finally, Edwin and Roberts [49] added symmetric external magnetic fields to this model and described what kind of wave modes such a system can guide with background parameters corresponding both to coronal and photospheric conditions. An extension to multi-layered plasmas was given by Ruderman [50], and multi-fibril prominence oscillations were modelled using the collective standing modes of a multi-layered Cartesian waveguide (Díaz et al. [51], Díaz and Roberts [52]) and coronal loop oscillations (Luna et al. [53]).

An important extension of Cartesian models was obtained by the inclusion of bulk background plasma motions in the equilibrium configuration. This addition helps capture a fundamental characteristic of the solar atmosphere, namely the wide-spread presence of flows in its various structures (such as spicules (Beckers [23], De Pontieu et al. [25,54]), macrospicules (Pike and Mason [55]), and X-ray and EUV jets (Shibata et al. [56])). The presence of shear flows in the model affects the properties of the guided waves and gives rise to, for example, the Kelvin–Helmholtz instability. One of the first steps towards the investigation of steady flows in a slab system was taken by Nakariakov and Roberts [57], where the central magnetic slab of a symmetric configuration also contained a background flow.

In Section 3, we provide an overview of recent advances made in the investigation of slab-like solar configurations by incorporating an asymmetric environment into the slab model in various ways, meaning that, as opposed to the "classical" symmetric model discussed above, we will allow for the regions surrounding the slab to be described by different equilibrium physical parameters. This can encompass a difference between, for example, the plasma pressure, the density, and the temperature on either side of the slab, or the magnetic field strength in the two environmental regions, or even a difference in the speed and/or direction of bulk background flows present in the external regions. Investigations using these slab geometries can provide a first approximation to model a plethora of solar atmospheric structures such as prominences, magnetic bright points, light walls, the boundary regions of coronal holes, the flank structure of coronal mass ejections, as well as several magnetospheric regions.

2.2.2. Cylindrical Models

Another popular model group is mainly used to approximate flux tubes in various parts of the solar atmosphere, but especially its outermost layer, the corona. This line of research first focused on straight cylindrical flux tubes of infinite length, motivated by providing a description of sunspots (Parker [58]) and further intense magnetic flux concentrations at supergranular boundaries (Defouw [59], Ryutov and Ryutova [60], Roberts and Webb [61]), as well as the effect of waves propagating along such structures on the corona and the solar wind (Wentzel [62], Wentzel [63]). Soon, the connection of MHD waves in magnetic flux tubes with flares (Zaitsev et al. [64]), as well as spicules and the question of atmospheric heating (Spruit and Roberts [65]) were examined, as well. As a logical extension of their study of magnetic slabs (see above), Edwin and Roberts [66] also worked on a magnetic flux tube model and summarised the possibilities of its application to both

photospheric flux tubes and coronal loops. In addition to the sausage and kink modes known from slab studies, they also described fluting modes (with azimuthal wavenumber $m \geq 2$).

In practice, the solar atmosphere contains such inhomogeneities that straight, untwisted cylinders of circular cross-sections are unlikely to exactly capture wave propagation in coronal loops. To take into account these possible differences from an idealised, fully axisymmetric system, e.g., Gu and Qiu [67], Ruderman [68], Erdélyi and Morton [69], Morton and Ruderman [70], and Aldhafeeri et al. [71] studied flux tubes with an elliptical cross-section. A different method of approximating an inhomogeneous environment using a flux tube model was developed by constructing models with annular magnetic cylinders to study kink and sausage waves without and then with the presence of twist in the annular structure (Mikhalyaev and Solov'ev [72], Mikhalyaev and Solov'ev [73], Carter and Erdélyi [74], Carter and Erdélyi [75]). In a similar configuration, Lopin [76] studied kink oscillations in semi-cylindrical shells.

Investigating whether the motions potentially driving the oscillations in cylindrical waveguides of the solar atmosphere are field-aligned (e.g., Dover et al. [77]) or tilted (Mackenzie Dover et al. [78], Skirvin et al. [79]) provides a different extension of flux tube studies, which improves our understanding of the waves guided and instabilities shown by solar jets such as spicules. For cylindrical, as well as slab models, another possibility is to focus on the gravitational stratification present within these narrower structures of the solar atmosphere (such as in Mather and Erdélyi [80] and Lopin and Nagorny [81]).

3. Results: MHD Waves in the Presence of Asymmetric Flows

Several avenues are open to us when it comes to expanding the complexity and applicability of traditionally Cartesian waveguide models, such as the inclusion of specific flow profiles [42], the study of standing waves [82,83], or the study of the resonant flow instability at an interface with a linear Alfvén speed profile [36]. The specific type of extension we review in the following section is that of keeping each of the regions of the slab system uniform and focusing on waves propagating along the slabs, but introducing various sources of asymmetry (plasma, magnetic field, flow speed) into the model. This recent line of study focusing on asymmetric slab systems was started by Allcock and Erdélyi [84] (see also Section 3.2), ultimately leading to a multi-slab model such as the one described in Allcock et al. [46] and Shukhobodskaia and Erdélyi [85] (see also Section 3.1). In the current section, we provide a summary of the method employed to derive the equation governing wave dispersion in such asymmetric systems, starting from the most general multi-layered model in this family. Then, we proceed to highlight the most important consequences of incorporating each different source of asymmetry into this model family, with a particular emphasis on the case when asymmetric background flows are present in the slab geometry. This summary of mainly analytical results is then followed by a discussion focused more on solar applications in Section 4.

3.1. Generalised Slab Model

Let us first consider a model of a plasma environment structured by an arbitrary number of interfaces with different homogeneous magnetic fields, temperatures, and densities, with each layer being subject to a bulk background flow of different magnitudes, illustrated in Figure 1 in Cartesian geometry. In this and the following similar figures, different background colours signify layers of different background densities, separated by vertical interfaces indicated as dashed black lines. Blue arrows denote the magnetic field lines, and thick red arrows indicate flows of various magnitudes.

Figure 1 shows the most general model within the multi-layered Cartesian slab family comprised of homogeneous layers separated by surfaces perpendicular to the x-direction. Various particular cases of this model, introduced in later sections, can serve to illustrate the effect of each of these different sources of asymmetry and provide a first approximation model of different solar atmospheric structures. We summarise the steps of deriving the

dispersion relation for magneto-acoustic waves propagating along the magnetic field in asymmetric slab systems for this most general case, then we focus on the properties of these waves and the applications of the results in the later sections.

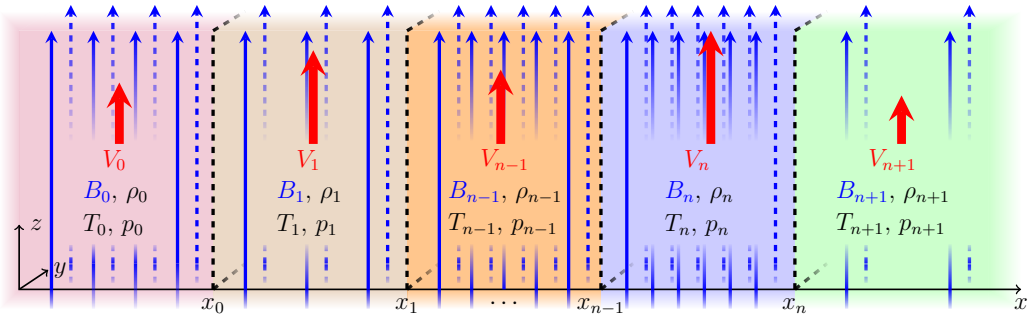

Figure 1. Generalised multi-layered Cartesian waveguide model including asymmetric flows. Structuring is present in the x-direction, while the system is infinite and non-stratified in the y- and z-directions.

First, let us, therefore, consider an infinite compressible inviscid structured static plasma permeated by magnetic fields $B(x)\,\hat{\mathbf{z}}$ and subject to background flows $V_{00}(x)\,\hat{\mathbf{z}}$ in the z-direction. In their simplest form, following the convention laid out in Allcock et al. [46], the different parameters of the plasma in equilibrium throughout each layer of this model can be summarised as

$$N(x) = \begin{cases} N_0, & \text{for } x < x_0, \\ N_1, & \text{for } x_0 \le x \le x_1, \\ \dots & \\ N_n, & \text{for } x_{n-1} \le x < x_n, \\ N_{n+1}, & \text{for } x \ge x_n, \end{cases} \tag{1}$$

where $N(x)$ can stand for any of the following parameters: plasma pressure, p, density, ρ, temperature, T, the z-component of the magnetic field, B_z, or the z-component of the background flow, V_{00}. The effects of gravity are ignored in this model. While in the solar atmosphere, gravity contributes to the stratification of atmospheric layers and has further effects on wave propagation, as is often the case with new directions explored in analytical studies, the multi-layered and asymmetric slab models described here constitute only a first step in describing an additional aspect of solar atmospheric structures, which influence wave propagation, and therefore, focus exclusively on this effect. The theory of asymmetric Cartesian waveguides is not yet developed in the area of studying magneto-acoustic gravity waves, and this limitation has to be kept in mind when applying the models laid out here.

It is assumed that the perturbations within the magnetic slab system are governed by the ideal MHD equations:

$$\begin{aligned} \rho \tfrac{D\mathbf{v}}{Dt} &= -\nabla p - \tfrac{1}{\mu_0}\mathbf{B} \times (\nabla \times \mathbf{B}), \\ \tfrac{\partial \rho}{\partial t} + \nabla \cdot (\rho \mathbf{v}) &= 0, \\ \tfrac{D}{Dt}\left(\tfrac{p}{\rho^\gamma}\right) &= 0, \\ \tfrac{\partial \mathbf{B}}{\partial t} &= \nabla \times (\mathbf{v} \times \mathbf{B}), \end{aligned} \tag{2}$$

where μ_0 is the magnetic permeability of the free space and γ is the adiabatic index. The plasma and magnetic parameters of the different media on either side of each discontinuity at $x = x_0, x_1, \dots, x_n$ need to be distributed so that the total pressure balance at each interface

is upheld, similarly to the classical configurations described by Roberts [47] and Edwin and Roberts [49]. This means that all across the slab system,

$$p_0 + \frac{(B_0)^2}{2\mu} = p_1 + \frac{(B_1)^2}{2\mu} = \ldots = p_n + \frac{(B_n)^2}{2\mu} = p_{n+1} + \frac{(B_{n+1})^2}{2\mu}. \tag{3}$$

Introducing the Alfvén ($v_{Aj} = B_j/\left(\mu\rho_j\right)^{0.5}$) and sound speeds ($c_j = \left(\gamma p_j\right)^{0.5}/\left(\rho_j\right)^{0.5}$) in the jth region, Equation (3) yields the following relation between these characteristic speeds of wave propagation and the density ratios of the layers for any two regions:

$$\frac{\rho_i}{\rho_j} = \frac{(c_j)^2 + \frac{1}{2}\gamma(v_{Aj})^2}{(c_i)^2 + \frac{1}{2}\gamma(v_{Ai})^2} \tag{4}$$

We linearised the governing Equation (2) by introducing a small, time-dependent perturbation to the temporally constant background quantities $N = N_j + N'$, where N_j is the background variable in region j and N' is the comparatively much smaller perturbation variable (customarily, $N'/N_j < 0.1$). After expanding the equations in this form, we neglected second- and higher order terms in the perturbation variables. Next, we sought plane wave solutions to the linearised governing equations of the form:

$$N'(\mathbf{x}, t) = \widehat{N}'(x)e^{i(k_y y + k_z z - \omega t)}, \tag{5}$$

where ω is the angular frequency and the y- and z-components of the wavenumber vector are k_y and k_z, respectively. Since these studies are focused on wave propagation solely along the magnetic field lines, in the z-direction, in the final step, $k_y = 0$ is applied to the equations derived. Substituting solutions (5) into the system of Equation (2) and combining the obtained equations, then enforcing the condition $k_y = 0$, the following ordinary differential equation for $\widehat{v}_x$ in each region is derived, representing transverse motions inside the magnetic slab:

$$\frac{d^2\widehat{v}_x}{dx^2} - m_j^2\widehat{v}_x = 0, \tag{6}$$

where

$$\begin{aligned} \left(m_j\right)^2 &= \frac{\left\{k^2 v_{Aj}^2 - \Omega_j^2\right\}\left\{k^2 c_j^2 - \Omega_j^2\right\}}{\left\{c_j^2 + v_{Aj}^2\right\}\left\{k^2 c_{Tj}^2 - \Omega_j^2\right\}}, \\ \left(c_{Tj}\right)^2 &= \frac{c_j^2 v_{Aj}^2}{\left(c_j^2 + v_{Aj}\right)^2}. \end{aligned} \tag{7}$$

In these equations and the following, the notation $k = k_z$ and $V_j = V_{j,z}$ is used, and the Doppler-shifted angular frequency in region j, $\Omega_j = \omega - k_z V_j$, is introduced due to the presence of flows. In any layer where the flow speed is set to zero in the subsequent models, the expression simply reduces to $\Omega_j = \omega$. Equation (6) can have certain special cases where the equation simplifies or contains a singularity. First, if $\Omega_j^2 = k^2 v_{Aj}^2$ or $\Omega_j^2 = k^2 c_j^2$, then the numerator in the corresponding m_j^2 coefficient becomes zero, leading to a linear solution to the ODE. The second special category is when a singularity is present in the denominator of m_j^2, with $\Omega_j^2 = k^2 c_{Tj}^2$. This leads to solutions where $\hat{v}_x = 0$ and $\hat{v}_z = 0$. In an ideal plasma, such as what the layers of this slab system are filled with, the magnetic field is frozen to the plasma, meaning that the magnetic field is not perturbed in this case, either. With no wave motions in either variable present, this case is discarded as a spurious solution. Next, it is assumed that perturbations must vanish at infinity, so that $\widehat{v}_x \to 0$ as $x \to \pm\infty$, and the further study focuses only on wave modes trapped in the slab system. Since the wave amplitudes decay exponentially at infinity, a general solution of Equation (6) is given by

$$\widehat{v}_x(x) = \begin{cases} P_0(\cosh m_0 x + \sinh m_0 x), & \text{for } x < x_0, \\ P_1 \cosh m_1 x + Q_1 \sinh m_1 x, & \text{for } x_0 < x < x_1, \\ \dots & \\ P_n \cosh m_n x + Q_n \sinh m_n x, & \text{for } x_{n-1} < x < x_n, \\ P_{n+1}(\cosh m_{n+1} x - Q_{n+1} \sinh m_{n+1} x), & \text{for } x_n < x. \end{cases} \tag{8}$$

Here, P_j and Q_j are constants with $j = 0, 1, \dots n, n+1$.

It may be shown that the amplitude of the total (plasma plus magnetic) pressure perturbation, $\widehat{p_T}(x)$, satisfies the following equation:

$$\widehat{p}(x) = \widehat{\mathbf{v}}'_{\mathbf{x}}(\mathbf{x}) \begin{cases} \Lambda_0/m_0, & \text{for } x < x_0, \\ \Lambda_1/m_1, & \text{for } x_0 < x < x_1, \\ \dots & \\ \Lambda_n/m_n, & \text{for } x_{n-1} < x < x_n, \\ \Lambda_{n+1}/m_{n+1}, & \text{for } x_n < x < x_n, \end{cases} \tag{9}$$

with

$$\Lambda_j = -\frac{i\rho_j \left\{ k^2 v_{Aj}^2 - \Omega_j^2 \right\}}{m_j \Omega_j}. \tag{10}$$

Using the notation above, the boundary conditions required for physical solutions, a.e., the continuity of the perturbed Lagrangian displacements and total pressures across all the interfaces, can be summarised as a system of $2n+2$ coupled homogeneous algebraic equations. Introducing the notation:

$$C_{j,i} = \cosh\left(m_j x_i\right), \qquad S_{j,i} = \sinh\left(m_j x_i\right) \tag{11}$$

shortens these equations considerably:

$$\begin{aligned} P_0\Omega_1(C_{0,0} + S_{0,0}) &= \Omega_0(P_1 C_{1,0} + Q_1 S_{1,0}), \\ \Lambda_0 P_0(C_{0,0} + S_{0,0}) &= \Lambda_1(Q_1 C_{1,0} + P_1 S_{1,0}), \\ \Omega_2(P_1 C_{1,1} + Q_1 S_{1,1}) &= \Omega_1(P_2 C_{2,1} + Q_2 S_{2,1}), \\ &\dots \\ \Omega_n(P_n C_{n,n} + Q_n S_{n,n}) &= \Omega_{n-1}(P_n C_{n,n-1} + Q_n S_{n,n-1}), \\ \Lambda_{n-1}(Q_{n-1} C_{n-1,n-1} + P_{n-1} S_{n-1,n-1}) &= \Lambda_n(Q_n C_{n,n-1} + P_n S_{n,n-1}), \\ \Omega_{n+1}(P_n C_{n,n} + Q_n S_{n,n}) &= \Omega_n P_{n+1}(C_{n+1,n} - S_{n+1,n}), \\ \Lambda_n(Q_n C_{n,n} + P_n S_{n,n}) &= \Lambda_{n+1} P_{n+1}(S_{n+1,n} - C_{n+1,n}). \end{aligned} \tag{12}$$

If we further define $Q_0 = P_0$ and $Q_{n+1} = -P_{n+1}$, then the obtained boundary conditions may be summarised in a more compact form as

$$\begin{aligned} \Omega_{j+1}\left(P_j C_{j,j} + Q_j S_{j,j}\right) &= \Omega_j P_{j+1}\left(C_{j+1,j} - S_{j+1,j}\right), \\ \Lambda_j\left(Q_j C_{j,j} + P_j S_{j,j}\right) &= \Lambda_{j+1} P_{j+1}\left(S_{j+1,j} - C_{j+1,j}\right) \end{aligned} \tag{13}$$

for $j = 0, 1, \dots, n-1, n$. The set of boundary conditions can also be rearranged into a $[2n+2] \times [2n+2]$ matrix and summarised as $\mathbf{M}\left(\mathbf{P_0},\ \mathbf{P_1},\ \mathbf{Q_1},\ \dots\ \mathbf{P_n},\ \mathbf{Q_n},\ \mathbf{P_{n+1}}\right)^T = \mathbf{0}$. In this matrix, each pair of rows expresses the continuity of the Lagrangian displacement (odd-numbered rows) and the total pressure (even-numbered rows) at a given interface. The first and last interfaces are described by slightly different conditions than the intermediate

ones, because they separate bounded regions from semi-infinite ones, in the latter of which the amplitude of the displacement perturbation must be evanescent.

Taking this into account, the first two rows will be given by:

$$\begin{array}{rclrclrcl} \mathbf{M}[1,1] &=& \Omega_1(C_{0,0}-S_{0,0}), & \mathbf{M}[1,2] &=& -\Omega_0 C_{1,0}, & \mathbf{M}[1,3] &=& -\Omega_0 S_{1,0}, \\ \mathbf{M}[2,1] &=& \Lambda_0(C_{0,0}+S_{0,0}), & \mathbf{M}[2,2] &=& -\Lambda_1 S_{1,1}, & \mathbf{M}[2,3] &=& -\Lambda_1 C_{1,1}. \end{array} \tag{14}$$

Similarly, the last two rows are

$$\begin{aligned} \mathbf{M}[2n+1,2n] &= \Omega_{n+1} C_{n,n} \\ \mathbf{M}[2n+1,2n+1] &= \Omega_{n+1} S_{n,n}, \\ \mathbf{M}[2n+1,2n+2] &= \Omega_n (S_{n+1,n} - C_{n+1,n}), \\ \mathbf{M}[2n+1,2n] &= \Lambda_n S_{n,n}, \\ \mathbf{M}[2n+1,2n+1] &= \Lambda_n C_{n,n}, \\ \mathbf{M}[2n+1,2n+2] &= \Lambda_{n+1}(C_{n+1,n} - S_{n+1,n}). \end{aligned} \tag{15}$$

For the intermediate layers $1 \leq j \leq n-1$, the general boundary conditions take the following form:

$$\begin{aligned} \mathbf{M}[2j+1,2j] &= \Omega_{j+1} C_{j,j} \\ \mathbf{M}[2j+1,2j+1] &= \Omega_{j+1} S_{j,j} \\ \mathbf{M}[2j+1,2j+2] &= -\Omega_j C_{j+1,j} \\ \mathbf{M}[2j+1,2j+3] &= -\Omega_j S_{j+1,j} \\ \mathbf{M}[2j+2,2j] &= -\Lambda_j S_{j,j} \\ \mathbf{M}[2j+2,2j+1] &= \Lambda_j C_{j,j} \\ \mathbf{M}[2j+2,2j+2] &= -\Lambda_{j+1} S_{j+1,j} \\ \mathbf{M}[2j+2,2j+3] &= -\Lambda_{j+1} C_{j+1,j}. \end{aligned} \tag{16}$$

All other matrix elements not explicitly given here are zero. This matrix is formally and structurally similar to the one detailed in Allcock et al. [46]; however, there are additional Ω_j multiplication factors contributing to the expressions, and due to the presence of the flows and the magnetic fields in each region, some of the coefficients expand into a more complex form.

Non-trivial solutions of the system of equations are found when the determinant of the matrix of boundary conditions is zero:

$$\det \mathbf{M} = 0. \tag{17}$$

Equation (17) serves as the general dispersion relation describing the propagation of linear MHD waves in a multi-layered Cartesian waveguide subject to steady flows, illustrated by Figure 1. The solutions to this equation expressed for the angular frequency, ω, as a function of the wavenumber, k, correspond to the eigenfrequencies of the system. Waves guided by simpler multi-layered waveguides, in the absence of flows, were investigated, e.g., in Allcock et al. [46], where, in a static equivalent of the generalised steady slab system presented here, each layer still contained plasmas of different densities, permeated by magnetic fields of different magnitudes. Further details of the frequencies and transverse velocity amplitude ($\hat{v}_x$) distributions of the eigenmodes were explored for a static multi-layered waveguide, where only a single layer contained magnetised plasma by Shukhobodskaia and Erdélyi [85]. These studies provide a solid basis for further future investigations relying on multi-layered Cartesian waveguides and their solar applications, as they already explore the effects of adding background density and then magnetic asymmetry to each layer. Comparing the results obtained for the equivalent configuration, which also contains steady background flows to these, will then provide an easy way to differentiate between

the consequences of asymmetries in the static background and those of the presence of asymmetric steady flows on the waves guided by each of these models.

It must be noted that, in general, the dispersion relation for multi-layered slab systems, Equation (17), is a highly complex equation, for which the solutions can be found employing numerical methods. However, in certain particular cases, as illustrated in the following sections, by, e.g., limiting the number of slabs, measuring the relative magnitude of the slab width compared to the wavenumber k, or utilising pre-existing information about the magnitude of the plasma-β parameters of the individual layers, analytical expressions for the eigenfrequencies may be found and help further our understanding of MHD waves guided by various slab systems.

3.2. Sources and Effects of Waveguide Asymmetry

Just as the most completely generalised multi-layered Cartesian waveguide model can be built up and studied step by step, the particular case of a single slab embedded between two external semi-infinite layers was constructed in a gradual process of incorporating ever-newer additional sources of asymmetry. Focusing on a single slab sandwiched between two environmental layers provides the not insignificant advantage of allowing us to simplify the dispersion relation in a number of limiting cases with relevant solar applications (such as the thin and wide slab or the high- and low-β limits). Through a combination of careful analytical study and extensive mapping of the parameter space by numerical methods, a more thorough understanding of the behaviour of eigenmodes in various slab systems has been gained. Additionally, just as we described for the case of the multi-layered models, gradually introducing different sources of asymmetry enables us to build a thorough understanding of the influence that each additional physical factor incorporated into the model has on the behaviour of eigenmodes and on the appearance of instabilities.

It is, therefore, worthwhile to first return to the most fundamental building block of single-slab models, namely that of the magnetised slab sandwiched between two, symmetric, non-magnetic layers of the environment, illustrated in Figure 2. Starting with this classical example, for the rest of this review of Cartesian studies, we must introduce a slightly different notation in order to remain compatible with the most widely used forms of the dispersion relation, as well as region and interface labelling in asymmetric and slab studies. Therefore, in the following models, the different parameters of the plasma in equilibrium in each layer will be referred to as

$$N(x) = \begin{cases} N_1, & \text{for } x < -x_0, \\ N_0, & \text{for } -x_0 \leq x \leq x_0, \\ N_2, & \text{for } x_0 < x, \end{cases} \tag{18}$$

where $N(x)$ can once again stand for any of the following parameters, when they are present: plasma pressure, p, density, ρ, temperature, T, the z-component of the magnetic field, B_z, or the z-component of the background flow, V_{00}. When introducing each model, simple illustrations of the distribution of background parameters will be included in order to clarify where magnetic fields and flows are present, and whether the environment is symmetric or not with respect to these parameters, as well as the plasma pressure.

With this new notation, for the classical slab model, there are no flows present in any region ($V_{1,0} = V_{0,0} = V_{0,0} = 0$), but each layer is magnetised, and the environment of the slab on its two sides is filled with the same kind of plasma, permeated by the same magnetic field ($p_1 = p_2 = p_e$, $B_1 = B_2 = B_e$). The dispersion relation for magneto-acoustic waves guided by this symmetric configuration is given by Equation (10) of Roberts [48]:

$$(k^2 v_{A0}^2 - \omega^2) m_e = \left(\frac{\rho_e}{\rho_0}\right) \omega^2 m_0 \begin{pmatrix} \tanh \\ \coth \end{pmatrix} (m_0 x_0), \tag{19}$$

where

$$\begin{aligned} m_0^2 &= \frac{(k^2 v_{A0}^2 - \omega^2)(k^2 c_0^2 - \omega^2)}{(k^2 c_{T0}^2 - \omega^2)(v_{A0}^2 + c_0^2)}, \\ m_e^2 &= \frac{(k^2 c_e^2 - \omega^2)}{c_e^2}, \end{aligned} \tag{20}$$

and the index 0 denotes quantities inside the central slab, while the index e refers to the parameters of the environmental regions. The solutions described by the top line of Equation (19) are sausage modes, while the bottom line containing the $\coth(m_0 x_0)$ term corresponds to kink modes. While the former leaves the central axis of the slab unperturbed and results in anti-phase perturbations of the slab boundaries, the latter does perturb the slab axis, but conserves the cross-sectional area and results in in-phase perturbations of the interfaces bordering the slab. Roberts [48] showed that both the kink and the sausage modes may be slow or fast waves, depending on whether their phase speed is smaller or larger than the internal sound or Alfvén speed. They may also take the form of surface waves (which are evanescent both inside and outside the slab) or body waves (which are evanescent outside the slab, but remain oscillatory inside the slab).

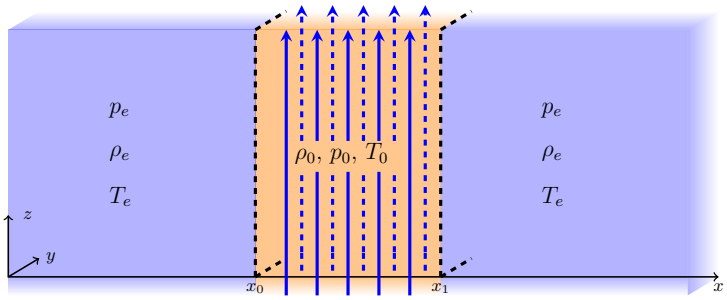

Figure 2. The model of a symmetric slab in a non-magnetic environment (figure based on Roberts [48]). Here, and in all the asymmetric slab systems that follow, stratification occurs in the x-direction only, while the system is generally infinite in the other two directions.

The first step in moving away from the "classical" symmetric models to the asymmetric slab geometries was taken by Allcock and Erdélyi [84], by allowing the two environmental regions of Roberts' model to be filled with plasmas of different densities and temperatures (illustrated in Figure 3), while keeping the total pressure balance (see Equation (3)) between all three regions. In this initial configuration, the slab itself is permeated by a vertical magnetic field, B_0, while the environment is non-magnetic $B_1 = B_2 = 0$, and there are no bulk background motions present in the system. The dispersion relation governing MHD waves in this asymmetric slab model is

$$\begin{aligned} \omega^4 m_0^2 &+ \frac{\rho_0}{\rho_1} m_1 \frac{\rho_0}{\rho_2} m_2 (k^2 v_{A0}^2 - \omega^2)^2 \\ &- \tfrac{1}{2} m_0 \omega^2 (k^2 v_{A0}^2 - \omega^2) \left(\frac{\rho_0}{\rho_1} m_1 + \frac{\rho_0}{\rho_2} m_2 \right) (\tanh(m_0 x_0) + \coth(m_0 x_0)) = 0, \end{aligned} \tag{21}$$

where, now,

$$\begin{aligned} m_0^2 &= \frac{(k^2 v_{A0}^2 - \omega^2)(k^2 c_0^2 - \omega^2)}{(k^2 c_{T0}^2 - \omega^2)(v_{A0}^2 + c_0^2)}, \\ m_j^2 &= \frac{(k^2 c_j^2 - \omega^2)}{c_j^2} \qquad \text{for } j = 1, 2. \end{aligned} \tag{22}$$

Beyond the explicit dependence of the angular frequencies on the external asymmetry present, one more factor immediately stands out about this new dispersion relation, namely that Equation (21) describes all eigenmodes guided by this configuration with one single, coupled equation, as opposed to the two separate equations valid for the symmetric eigenmodes seen in Equation (19). This mathematical property manifests physically in the fact that the asymmetric eigenmodes show a mixed character instead of a purely kink or purely sausage mode behaviour, which is why they are referred to as quasi-kink and

quasi-sausage modes instead. Since, in several follow-up studies (such as Allcock et al. [46]), it was shown that asymmetric slab systems are, in general, characterised by the presence of quasi-sausage and quasi-kink eigenmodes instead of purely kink or sausage oscillations, it is worthwhile to discuss their fundamental properties in some detail next, which may be used for the purposes of SMS (Lopin and Nagorny [86], Li et al. [87]).

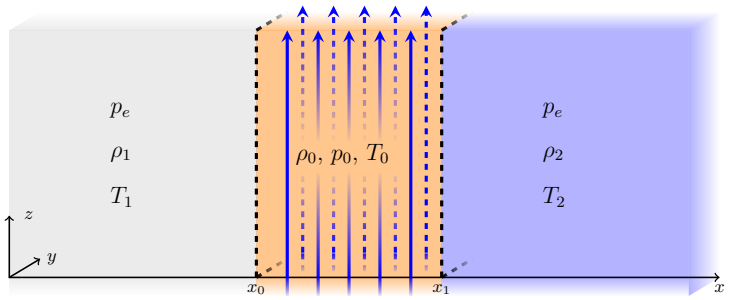

Figure 3. The model of a magnetic slab in an asymmetric non-magnetic environment (based on Figure 1 of Allcock and Erdélyi [84]). To keep the external pressures balanced, in accordance with Equation (3), they take the same value ($p_1 = p_2 = p_e$), although the corresponding combinations of density and temperature may be different.

In the case of the asymmetric eigenmodes, the transverse velocity shows an asymmetric distribution across the slab and its environment, which can be observed as different amplitudes of oscillation at the two interfaces on its boundaries. This effect is shown in Figure 4, in which the solid black curve displays numerical results obtained for the transverse velocity perturbation ($\hat{v_x}(x)$) as a function of the transverse spatial coordinate, x, overlaid on an illustration of an asymmetric system containing a dense and strongly magnetised slab (described by the following set of background parameters: $v_{A0} = 0.7c_0$, $v_{A1} = 0.2c_0$, $v_{A2} = 0.1c_0$, $c_1 = 2.2279c_0$, $c_2 = 1.8742c_0$, $\rho_1/\rho_0 = 0.28$, and $\rho_2/\rho_0 = 0.4$).

Figure 4a shows a slow quasi-sausage surface mode; Figure 4b is a slow quasi-kink surface mode; Figure 4c displays a fast quasi-sausage body mode of order one (a.i., having only one node inside the slab); Figure 4d depicts a fast quasi-kink body mode of order one. Figure 4a,b show solutions in a narrow slab (with $kx_0 = 0.685$), but Figure 4c,d display solutions from a wider slab ($kx_0 = 2.790$).

Another major difference between symmetric eigenmodes and their asymmetric counterparts is that the unperturbed magnetic surface of quasi-sausage modes and the minimally perturbed magnetic surface for quasi-kink modes becomes shifted away from the geometric centre of the slab, where it would be found for symmetric sausage and kink modes. The properties of the asymmetric eigenmodes, as well as their dependence on the external density and magnetic field ratios, were further investigated by Allcock and Erdélyi [84,88], Zsámberger et al. [89], Oxley et al. [82,83], and Zsámberger and Erdélyi [90]. These studies proceed to provide a set of new tools to be used for the purposes of solar magnetoseismology based on waveguide asymmetry. Allcock and Erdélyi [88] provides the initial derivation and definition of the additional quantities that need to be found for each slab system to exploit the potential new SMS tools offered by asymmetric models. Firstly, the amplitude ratio method relies on the difference of the amplitudes in the velocity or Lagrangian displacement perturbation at the two interfaces delimiting the slab due to the presence of external asymmetry. The amplitude ratio, R_A, is defined in the form of a fraction, where the numerator is the oscillation amplitude on the left-hand-side boundary of the slab (at $-x_0$) and the denominator is the same quantity, but measured at the right-hand-side interface (at x_0). This quantity is derived using the dispersion relation of the configuration and the solutions for the perturbed velocities (see, e.g., Equation (8) for the multi-layered slab). Using the derived expressions and measuring the amplitude ratio in observations makes it possible to estimate a "missing" parameter in the system, such as the Alfvén speed estimates obtained for chromospheric fibrils in Allcock et al. [46]. An additional tool to use can

be the minimum perturbation shift method also laid out in Allcock and Erdélyi [88]. Here, the minimum perturbation shift, Δ_{min}, is defined as the displacement (from the central line of the slab) of the position of minimum wave power inside an asymmetric magnetic slab. Similar to the amplitude ratio, this quantity can also be derived analytically from the velocity solutions and the dispersion relation, and then measured observationally to then determine one unknown parameter of the system. Both R_A and Δ_{min} are different expressions for quasi-sausage and quasi-kink modes, but they each rely on the asymmetry introduced into the displacement/velocity distribution introduced into the eigenmodes by the differences in the plasma and magnetic parameters in the environmental regions of the slab system. As mentioned, Allcock et al. [46] demonstrated the application of these tools as a proof of concept, using MHD waves observed in chromospheric fibrils. The analytical part of these methods was then extended to a slab system containing both plasma and magnetic asymmetry by Zsámberger and Erdélyi [90]. While these studies focused on propagating waves, Oxley et al. [82,83] investigated standing waves in the presence of only plasma asymmetry, and then considering both plasma and magnetic asymmetries in the model. These studies provided analytical expressions for the frequency ratio of the first harmonic to the fundamental mode, as well as the relative amplitude difference between the two sides of the slab (which functions similarly to the amplitude ratio method described earlier). They also showed the relative frequency and amplitude difference in an asymmetric system compared to a symmetric slab to highlight the importance of selecting the appropriate model for conducting SMS studies.

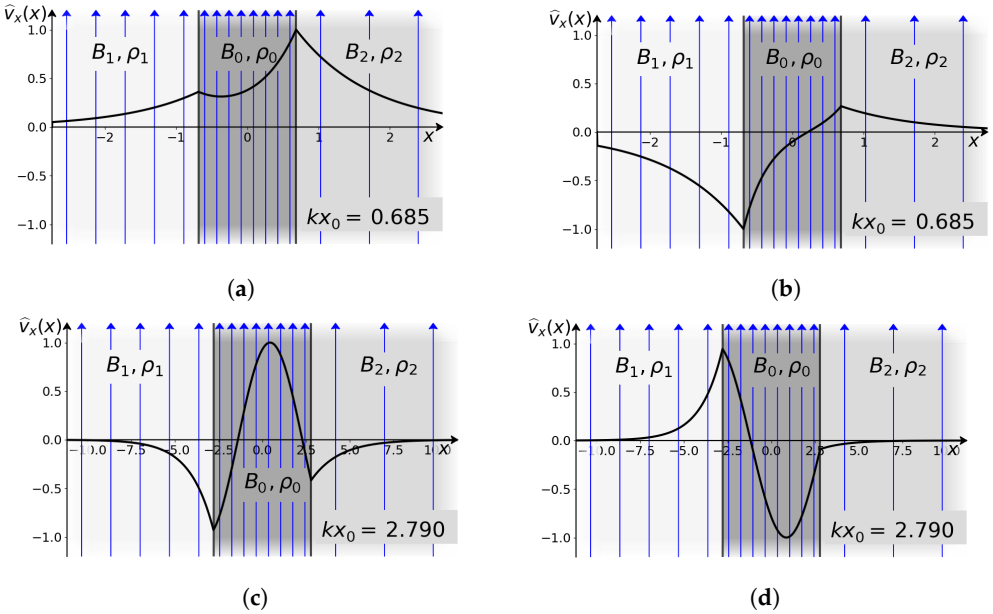

Figure 4. The transverse velocity perturbation amplitude of eigenmodes in an asymmetric magnetic slab, adapted from Figure 4 of Allcock et al. [46]. Panels (**a**,**b**) show a quasi-kink- and a quasi-sausage surface mode, respectively, in a thin slab. Panels (**c**,**d**) depict a quasi-kink and a quasi-sausage body mode in a wider slab. In all four cases, the slab is strongly magnetised and embedded in a rarefied asymmetric environment.

Beyond the properties of asymmetric eigenmodes in general, Allcock and Erdélyi [84] also describes other consequences of incorporating density asymmetry into the external parameters. These effects can also be observed in more complex asymmetric single-slab systems, which incorporate different magnetic fields and flows, but including a density asymmetry by itself can already be sufficient to make them apparent. Especially noteworthy among these effects is that, generally, surface modes are more strongly affected by introducing a difference between the physical parameters of the two environmental regions than body modes tend to be. Furthermore, in wide slabs (when $kx_0 \gg 1$), the phase speeds

of a pair of quasi-sausage and quasi-kink surface modes no longer tend to the same value, as they would in a symmetric system (see Roberts [48], Edwin and Roberts [49]), but rather, to two distinct speeds. On the other hand, in thin slabs ($kx_0 \ll 1$), the fast quasi-sausage surface mode may not exist as a trapped oscillation due to the presence of a divergence in the external sound speeds. It should be noted that, for the purposes of the analytical investigation of the behaviour of eigenmodes in the limits listed above, Equation (21), the full dispersion relation, can be decoupled and transformed into a similar pair of equations for quasi-kink and quasi-sausage modes as Roberts [48] and Edwin and Roberts [49] derived for purely kink and sausage modes (see, e.g., Equation (19) above). This requires the introduction of the so-called weak asymmetry limit, where it is assumed that the plasma (and when applicable, magnetic and flow) parameters when the system is in equilibrium are of the same order of magnitude on either side of the slab. Detailed steps of this transformation are included in Allcock [91]. The decoupled dispersion relation obtained this way significantly simplifies the analytics of the problem and makes direct comparisons with the corresponding symmetric cases possible, while still remaining notably accurate, based on the investigation carried out by Zsámberger et al. [92].

How these effects of asymmetry in the properties of the plasma filling the environmental regions are then compounded by introducing an external magnetic asymmetry into the model were investigated in detail by, e.g., Zsámberger and Erdélyi [93] with a model illustrated in Figure 5. Now, all three regions are permeated by magnetic fields of different strength, and the properties of the plasma filling each layer are all different from one another, including the plasma pressure itself ($p_1 \neq p_0 \neq p_2$). As mentioned before, the eigenmodes of this model are quasi-kink and quasi-sausage waves, which are both governed by one single dispersion relation:

$$\begin{aligned} &2m_0^2\left(k^2v_{A1}^2-\omega^2\right)\left(k^2v_{A2}^2-\omega^2\right)+2\tfrac{\rho_0}{\rho_1}m_1\tfrac{\rho_0}{\rho_2}m_2\left(k^2v_{A0}^2-\omega^2\right)^2 \\ &+\rho_0m_0\left(k^2v_{A0}^2-\omega^2\right)\left[\tfrac{m_2}{\rho_2}\left(k^2v_{A1}^2-\omega^2\right)\right. \\ &\left.+\tfrac{m_1}{\rho_1}\left(k^2v_{A2}^2-\omega^2\right)\right]\left[\tanh\left(m_0x_0\right)+\coth\left(m_0x_0\right)\right]=0, \end{aligned} \tag{23}$$

where

$$m_j^2=\frac{\left(k^2v_{Aj}^2-\omega^2\right)\left(k^2c_j^2-\omega^2\right)}{\left(v_{Aj}^2+c_j^2\right)\left(k^2c_{Tj}^2-\omega^2\right)}, \qquad \text{for } j=0,1,2. \tag{24}$$

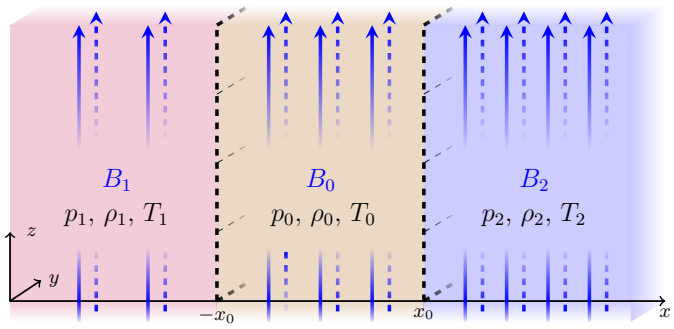

Figure 5. The model of a magnetic slab in an asymmetric magnetic environment, where both the plasma parameters and the magnetic field strength may take different values in the two external regions (adapted from Figure 1 of Zsámberger et al. [89]).

As described by Zsámberger et al. [89], the presence of different external magnetic fields provides a new source of influence on the eigenmodes, which can compete with the effects of the density asymmetry, e.g., in determining which direction and how far the surface of minimum or zero perturbation is shifted for quasi-kink and quasi-sausage modes, respectively. In addition to the consequences on the phase speeds of the modes described

in the externally non-magnetic asymmetric case, in the fully magnetic asymmetric slab system, there are additional cut-off speeds present. Firstly, these result in a vastly more complex problem with far more possible orderings of the external and internal characteristic speeds (Alfvén, sound, and tube speeds), splitting the problem into several different cases in which the waveguide will be able to support a different set of fast or slow, body or surface modes. Secondly, the presence of the different external magnetic fields introduces additional cut-off frequencies both when compared to the symmetric magnetic case studied by Edwin and Roberts [49] and to the asymmetric non-magnetic case described by Allcock and Erdélyi [84]. Zsámberger and Erdélyi [93] showed that some of the surface and body modes now may not exist as trapped oscillations in a thin slab, and the frequency bands where body modes occur can be split into two or three separate bands by the additional cut-off frequencies stemming from the presence of the magnetic asymmetry.

After the summary of the consequences of different sources of waveguide asymmetry provided above for stationary models, now, we can turn our attention to single-slab models, which also incorporate steady flows in one or more layers and focus on the effects of the flow asymmetry itself on the frequencies of the eigenmodes and the appearance of instabilities.

3.3. Flow Asymmetry

Incorporating bulk background motions in one or even several layers of the slab model makes it possible to take further physical effects into consideration beyond the ones described already in relation to static models and potentially increase the scope of applicability of this model family. Once the presence of flows is considered, a fundamental difference that emerges compared to static models is the possibility of shearing motions in the configuration, which, in turn, can lead to the onset of the Kelvin–Helmholtz instability under the right circumstances. Therefore, while the solutions to the dispersion relations of static slab systems always yielded stable results, the stability of waves guided by steady slabs must also be investigated. An additional effect of the presence of background flows can be a shift in the phase speed of the waves and the cut-off frequencies separating trapped oscillations from leaky modes—even in the case of a symmetric steady slab model (see, e.g., Nakariakov and Roberts [57]). Depending on the exact setup of the model, other phenomena may come into play as well due to the background flows, such as negative energy wave instabilities or resonant flow instabilities (see Taroyan and Ruderman [94] and Ryutova [95]).

The symmetric slab model incorporating bulk background motions discussed by Nakariakov and Roberts [57] was generalised for an asymmetric, externally non-magnetic slab system by Barbulescu and Erdélyi [96], who even provided a simple demonstration of how to use this mode to estimate the density ratio of ejecta in the flank region of a coronal mass ejection (CME) compared to the general background of the plasma environment in the solar corona. This slab model then gained a further extension in Zsámberger et al. [92] for an even more generalised case, which combines both density and magnetic asymmetry in the external quantities with the inclusion of a background flow in the central region. While this brings us closer to an accurate description of CME flank regions, we must bear in mind that the slab models have their limits stemming from their basic assumptions. While including gravity in the models, for example, would further improve accuracy, these steps in modelling still represent potential improvements over the previously suggested single interface interpretation (Foullon et al. [97]). The new configuration is depicted in Figure 6. Keeping in mind that, due to the presence of the flow, the Doppler-shifted frequency ($\Omega = \omega - kV_0$) replaces the pure angular frequency in the central region, the dispersion relation governing MHD waves in this model can be written as

$$2\frac{\rho_0}{\rho_1}m_1\frac{\rho_0}{\rho_2}m_2(k^2v_{A0}^2-\Omega^2)^2+2m_0^2(k^2v_{A1}^2-\omega^2)(k^2v_{A2}^2-\omega^2)+\rho_0 m_0$$
$$(k^2v_{A0}^2-\Omega^2)\left[\frac{m_2}{\rho_2}(k^2v_{A1}^2-\omega^2)+\frac{m_1}{\rho_1}(k^2v_{A2}^2-\omega^2)\right][\tanh(m_0x_0)+\coth(m_0x_0)]=0, \quad (25)$$

where, in this case,

$$\begin{aligned} m_0^2 &= \frac{(k^2 v_{A0}^2 - \Omega^2)(k^2 c_0^2 - \Omega^2)}{(c_0^2 + v_{A0}^2)(k^2 c_{T0}^2 - \Omega^2)}, \quad \text{and} \\ m_j^2 &= \frac{(k^2 v_{Aj}^2 - \omega^2)(k^2 c_j^2 - \omega^2)}{(c_j^2 + v_{Aj}^2)(k^2 c_{Tj}^2 - \omega^2)} \quad \text{for } j = 1, 2. \end{aligned} \tag{26}$$

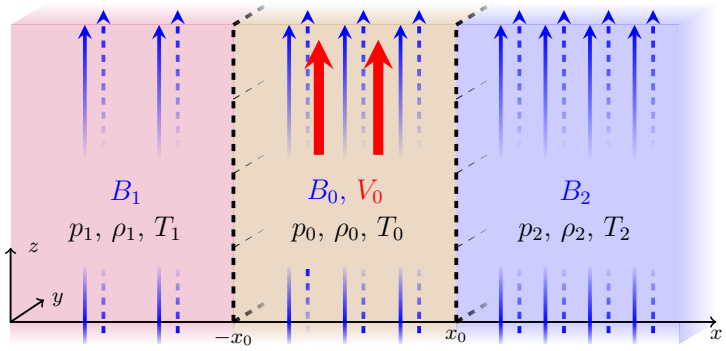

Figure 6. The model of an asymmetric magnetic slab system similar to the one depicted in Figure 5, keeping both plasma and magnetic asymmetries present, but now also including a steady flow in the central region (based on Figure 1 of Zsámberger et al. [92]).

This example shows and other particular cases (see, e.g., Allcock et al. [46]), as well as the generalised multi-layered case described in Section 3.1 confirm that, even once background flows are built into the model, the dispersion relation still does not decouple into separate equations for purely sausage or purely kink modes, but instead, it still describes quasi-sausage and quasi-kink modes together. To facilitate a better analytical understanding of the problem, it is possible to consider only the so-called weak asymmetry case, when the external densities and magnetic fields are not the same, but also not drastically different from one another. In this case, it becomes possible to decouple the dispersion relation and obtain a separate equation for both sausage- and kink-type modes, which will be formally similar to the relation valid for the symmetric case, with

$$(k^2 v_{A0}^2 - \Omega^2)\left(\frac{\rho_0}{\rho_1}\frac{m_1}{(k^2 v_{A1}^2 - \omega^2)} + \frac{\rho_0}{\rho_2}\frac{m_2}{(k^2 v_{A2}^2 - \omega^2)}\right) + 2m_0 \left\{ \begin{array}{c} \tanh \\ \coth \end{array} \right\}(m_0 x_0) = 0. \tag{27}$$

Using this decoupled (approximate) dispersion relation, Zsámberger et al. [92] provided analytical solutions for the eigenmodes that may be present in a thin slab and, based on these, determined a relation between the threshold flow speed required for the onset of the KHI and the characteristic speeds and densities of the model for each of the possible modes. Their further numerical study showed good agreement between the thin slab and the weak asymmetry solutions, as well as the solutions of the full and exact dispersion relation. The numerical results further highlighted some interesting consequences of the shifted phase speeds and cut-off frequencies influenced by the presence of the central flow. Multiple possible regions of instability were found, with different eigenmodes becoming unstable for different ranges of the Alfvén Mach number ($M_{A0} = V_0/v_{A0}$, which describes the relative magnitude of the flow speed compared to the Alfvén speed in the central slab).

Figure 7 illustrates this behaviour, with the real part of the phase speeds plotted in blue and the two branches of the imaginary part (symmetric about the $\omega/kv_{A0} = 0$ line) shown in red. The region above the $c_1 = c_2$ line in the case of Figure 7a, and above the line indicating c_2 in the case of panel b, would contain only leaky solutions (with $m_1^2 < 0$, or $m_2^2 < 0$, or both), which were not included in the references studied. A version of these results displaying a larger segment of the $M_{A0} - \omega$ parameter space appeared

in Zsámberger et al. [92], which we reproduce here to better showcase one particular consequence of introducing flow asymmetry into the environment of the slab.

Figure 7a shows the waves propagating in a symmetric steady slab system described by the following set of plasma parameters in equilibrium: $c_0 = 0.8v_{A0}$, $c_1 = c_2 = 1.51v_{A0}$, $v_{A1} = v_{A2} = 0.9v_{A0}$, and $\rho_1/\rho_0 = \rho_2/\rho_0 = 0.5$. Next to it, Figure 7b shows how the phase speeds and stability of the solutions change when plasma and magnetic asymmetry are introduced into the steady slab system, with $c_0 = 0.8v_{A0}$, $c_1 = 1.51v_{A0}$, $c_2 = 1.33v_{A0}$, $v_{A1} = 0.9v_{A0}$, $v_{A2} = 0.9v_{A0}$, $\rho_1/\rho_0 = 0.5$, and $\rho_2/\rho_0 = 0.6$. In both cases, the slow quasi-kink modes propagate with a speed close to the external tube speeds and become strongly affected by the flow. They remain stable solutions up to quite high flow speeds, but beyond $M_{A0} = 2.5$, the forward- and backward-propagating modes are shifted enough by the flow to meet at the same phase speed value, which leads to the onset of the KHI. This is, however, not the lowest possible value of M_A, where an instability can occur. In Figure 7a, the fast sausage modes can become unstable for an Alfvén Mach number of $M_{A0} \approx 2$. However, once their propagation speed exceeds the external sound speed ($c_e = c_1 = c_2$ for this symmetric case), they show a sharp cut-off, because they are shifted into the leaky regime. The inclusion of density and magnetic asymmetry in Figure 7b creates an even more restrictive environment, where no unstable trapped solutions exist at all in the same M_{A0} regime due to the divergence of the external sound speeds. It should also be noted that a far lower flow speed may be enough to give rise to unstable solutions and, therefore, render the whole slab system unstable, as using a high-resolution grid to solve the dispersion relation revealed a third possible KHI-unstable flow speed regime at around $M_A = 1.5$ (shown in the inlets of Figure 7a,b).

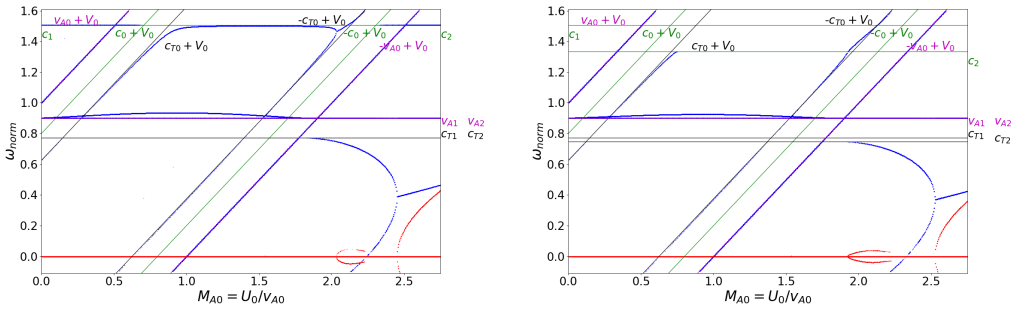

(**a**) (**b**)

Figure 7. Solutions of the full dispersion relation (Equation (25)) in (**a**) a symmetric slab and in (**b**) a weakly asymmetric slab.

An additional source of extended parameter regimes of instability can be an asymmetry in the flow speeds themselves within a slab system. This problem was studied by Zsámberger et al. [98], who analysed MHD wave propagation and the KHI in the model of a magnetic slab surrounded by a non-magnetic, asymmetric plasma environment, which, additionally, contained steady flows of different magnitudes in the external regions, illustrated in Figure 8. The full (non-decoupled) dispersion relation of this configuration is given by

$$m_0^2\Omega_1^2\Omega_2^2 + \frac{\rho_0}{\rho_1}m_1\frac{\rho_0}{\rho_2}m_2(k^2v_{A0}^2 - \omega^2)^2 - \frac{1}{2}m_0(k^2v_{A0}^2 - \omega^2)\left(\frac{\rho_0}{\rho_1}m_1\Omega_2^2 + \frac{\rho_0}{\rho_2}m_2\Omega_1^2\right)(\tanh(m_0x_0) + \coth(m_0x_0)) = 0, \tag{28}$$

where

$$m_0^2 = \frac{(k^2v_{A0}^2 - \omega^2)(k^2c_0^2 - \omega^2)}{(c_0^2 + v_{A0}^2)(k^2c_{T0}^2 - \omega^2)},$$
$$m_j^2 = k^2 - \frac{\Omega_j^2}{c_j^2} \quad \text{for } j = 1, 2. \tag{29}$$

Due to the presence of two different flows in two layers of this model, two different Doppler-shifted frequencies enter into the equation governing MHD wave behaviour in the slab: $\Omega_j = \omega - kU_j$ for $j = 1, 2$. These two flow speeds may point in the same direction or describe movement in opposite directions on the two sides of the slab, acting together to occasionally create far more favourable conditions for instabilities to appear than a single flow of similar speed would.

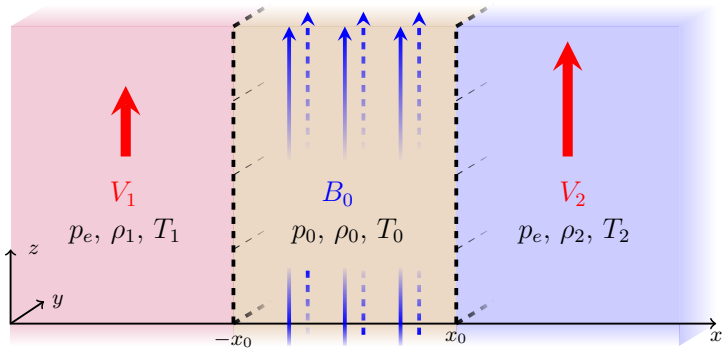

Figure 8. The model of a magnetic slab surrounded by different flows in its asymmetric non-magnetic plasma environment (based on Figure 1 of Zsámberger et al. [98]). Similar to the case illustrated in Figure 3, the external pressures are the same, while the other parameters are allowed to break symmetry.

The panels of Figure 9 help illustrate this effect, where the phase speed of the waves is plotted as a function of the changing right-hand-side Alfvén Mach number (M_{A2}), for a different fixed value of M_{A1} in each panel in a thin slab. In each of these panels there is a "central oval" region in which the solutions are stable. This region does not fall exactly in the centre of the diagrams, but rather, it is shifted based on both the flow speeds chosen and the relative difference between these two speeds. Outside the "central oval", even at relatively small values of the right-hand-side flow, the phase speeds of the forward- and backward-propagating surface waves meet, resulting in the onset of the KHI. This happens on both sides of the central region; however, due to the asymmetric flow speeds, the KHI onset happens at different values of M_{A2} on the negative half of the M_{A2} axis than on the positive side. The extent of the central stable region was shown to depend on the dimensionless slab width in the same study, leading to the conclusion that all else being the same, the wider a slab is, the larger the critical value of M_{A2} required for the KHI onset becomes.

While the inclusion of bulk background flows in any region of the slab system already has a strong effect on the waves guided by the configuration (changing both the types and frequencies of modes supported as trapped oscillations, as well as stability limits), investigating asymmetric flows specifically also causes a significant lowering of the requirements for each flow speed needed for making the system vulnerable to the KHI possible.

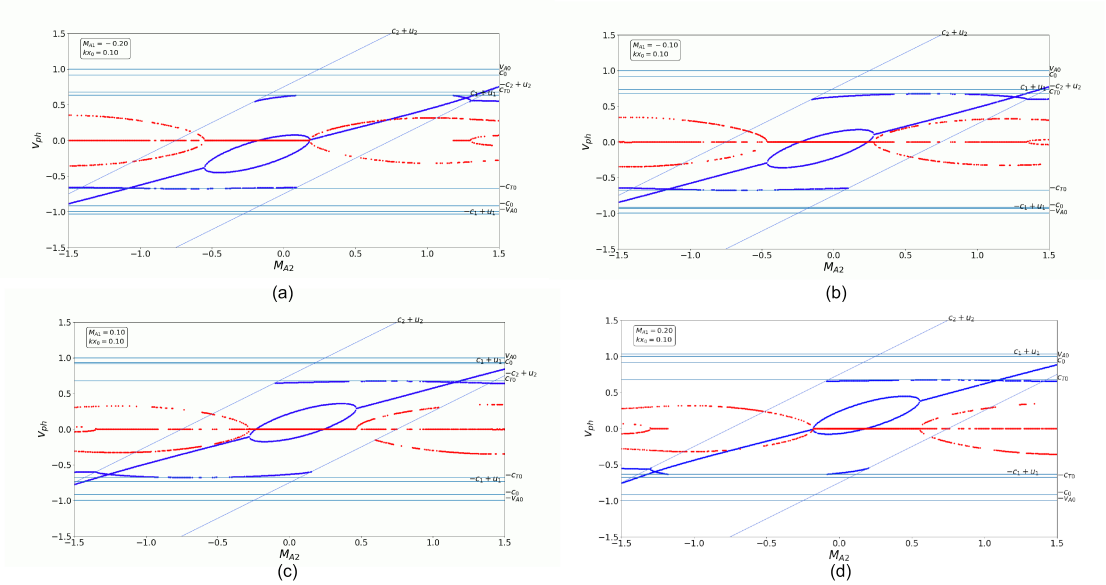

Figure 9. Phase speeds of trapped oscillations in a magnetic slab as a function of the external Alfvén Mach number on the right-hand side, in a slab of fixed width, kx_0. Through panels (**a**–**d**), the left-hand-side Alfvén Mach number increases from $M_{A1} = -0.2$ to $M_{A1} = +0.2$, shifting the central stable region with it. Source: Figure 5 of Zsámberger et al. [98].

4. Discussion: Solar Applications

Several potential applications of different asymmetric slab systems have been suggested in a solar context. These can be divided based on two deciding factors: were static or steady slab models used, and what was the spatial extent of the suggested application in the solar atmosphere or the Earth's magnetosphere? Based on the first criterion, Figures 10 and 11 provide an illustration of suggested or completed SMS applications of recently developed asymmetric or multi-layered Cartesian waveguide models for static and steady equilibria, respectively. For completeness, we note that further details and full-resolution images are available in the publications relevant to each specific model listed in these overview figures. Of course, these suggested applications are not exclusive to any of these models; they are merely intended to provide examples of space plasma environments where each model captures a certain physical process essential to the understanding of said solar or magnetospheric environment.

In order of appearance, the first line in Figure 10 connects the analytical model of a static, externally non-magnetic asymmetric slab system (studied by Allcock and Erdélyi [84]) to the SMS investigation of fibrils in the solar chromosphere carried out by Allcock et al. [46]. This example already highlights a point we shall discuss later: the importance of the choice of model. The same observations referenced here were first interpreted as oscillating flux tubes showing a superposition of sausage and kink modes, finding a modal oscillation period of 120 s (Morton et al. [99] and Mooroogen et al. [100]), whereas the asymmetric slab model discussed them in terms of single quasi-kink or quasi-sausage modes, focusing on a different aspect of the available waveguide information. For both approaches, the high spatial resolution of 150 km on the solar surface was necessary and barely sufficient, providing 10–20 pixels across each fibril for these studies (Allcock et al. [46]).

In the second line of Figure 10, a similar theoretical model is shown. However, while the infinite, invariant nature of the slab system is kept in the y-direction, this model is closed in the z-direction for the study of standing waves. This can be a promising interpretation of a prominence: a region of cooler and denser plasma embedded between two slightly different regions of the hot solar corona with lengths of 60–600 Mm along the magnetic field lines, widths of 3–10 Mm across, and heights of 10–100 Mm (Priest [101], Zsámberger and Erdélyi [102], Oxley et al. [82]). Both small- and large-amplitude oscillations have been observed in prominences. While the lifetime of a prominence can be as

long as several days, the oscillation periods detected typically range from a few minutes to over an hour (Arregui et al. [103]).

The externally non-magnetic model was generalised into a multi-layered waveguide (remaining infinite in the z-direction for the study of propagating waves) by Shukhobodskaia and Erdélyi [85], who suggested its application to magnetic bright points and their surrounding intergranular lanes and granular cells in the photosphere of the Sun. This pair of modelling and observations is displayed in line 3 of Figure 10. Magnetic bright points themselves are short-lived flux concentrations, with the majority of them having lifetimes on the scale of a few minutes only. Their lifetimes are related to their size, which ranges from tens to hundreds of kilometres Abramenko et al. [104], although their perpendicular extent and shape can vary greatly (Bovelet and Wiehr [105]).

The remaining lines of this figure deal with the externally magnetic and asymmetric counterparts of each of the three models above. Line 4 shows the asymmetric magnetic slab and its suggested application to coronal plumes or boundary regions of coronal holes and the quiet solar atmosphere (see Zsámberger and Erdélyi [102]). The bright, mostly radial rays forming the plumes follow the lines of the magnetic field and can remain unchanged for days. They are large-scale structures, with a base diameter of about 30 Mm and extending out into the solar atmosphere for hundreds of Mms (DeForest and Gurman [106], Poletto [107]). Line 5 then shows the closed, standing wave version of the previous model discussed as a possibility to model light bridges (light walls) separating sunspots into two umbral cores in Oxley et al. [83]. Finally, in line 6, the fully magnetised multi-layered Cartesian model described in Allcock et al. [46] is shown. This geometry, containing an arbitrary number of magnetised plasma domains, can also be tailored to approximate the structure of light bridges, as it can often happen that a big sunspot is divided up into more than two umbral cores by several light bridges. The size of an individual light bridge can range from one to several arcseconds on the solar surface (approximately seven hundred to a few thousand kilometres), and their lifetimes are measurable on the scale of a day or less, after which the sunspot cores they lie between either merge or separate fully (Vazquez [108], Sobotka et al. [109], Lagg et al. [110]).

A similar summary of steady slab models is provided in Figure 11. The first line here introduces the model of an externally non-magnetic, asymmetric magnetic slab containing a steady flow in the central region. Barbulescu and Erdélyi [96] derived the properties of this waveguide and described its application to CME flank regions. Using the original parameters measured by Foullon et al. [111], this investigation, as well, focused on a small segment of a larger scale coronal mass ejection, with a flank layer width of approximately 4 Mm.

Next, in line 2 of Figure 11, the slab system incorporates an external flow asymmetry instead, which may be useful in studying the fibrillar structure in the penumbrae of sunspots closely connected to the Evershed flow (Tsiropoula [112], Borrero and Ichimoto [113]). Instead of the external flow asymmetry, line 3 of Figure 11 shows a model that focuses on the external magnetic asymmetry, while keeping a central background flow in the slab, which may be used to interpret waves and instabilities in solar spicules.

Line 4 of Figure 11 unifies the two preceding approaches, showing a fully magnetised slab system with external flow and magnetic asymmetries included (Allcock et al. [46]). This approach can refine the modelling of a magnetic bright point and its asymmetric intergranular environment containing downflows of various speeds. Line 5 provides a further addition to this, showing the most generalised case of a steady asymmetric one-slab system, which can also be applied to, e.g., the triad of the Earth's magnetopause, magnetosheath, and bow shock regions (Turkakin et al. [114], Allcock et al. [46], Nenovski [115]).

Finally, line 6 of Figure 11 displays the furthest generalised case of an asymmetric multi-layered steady Cartesian waveguide presented at the beginning of Section 3, which, just like its static counterparts, can serve as a refinement of the slab modelling of multiple light bridges, or the extended environment of MBPs.

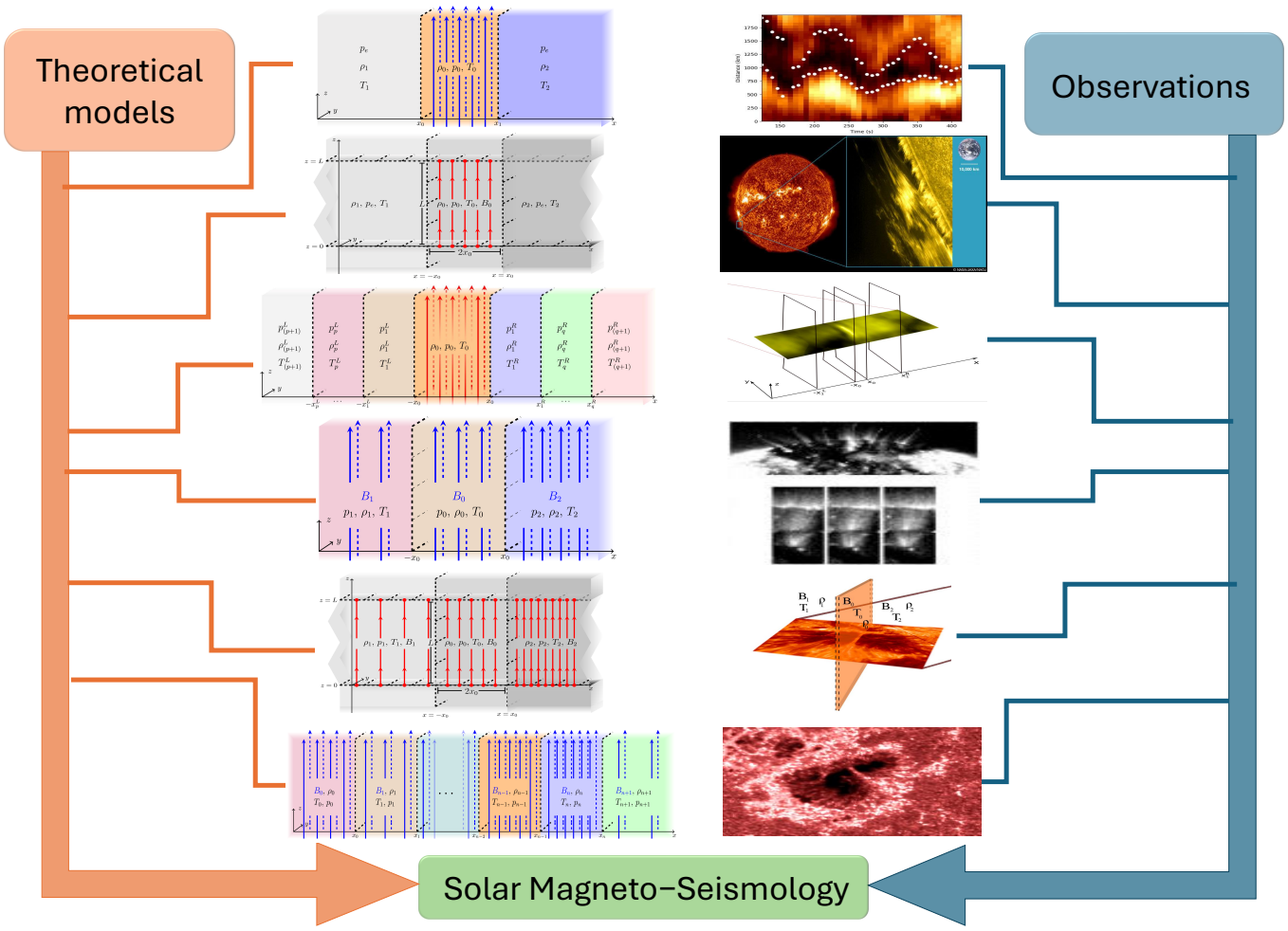

Figure 10. The family of recent static asymmetric slab models and their potential applications to observable structures in solar magneto-seismology.

The second categorisation of asymmetric static and steady slab models of the solar atmosphere is based on spatial scales and divides said applications into two main groups: the global stratification of the solar atmosphere and local structures within it. Zsámberger and Erdélyi [102] put forward several of these various solar environments for further study as static magnetic slab models embedded in an asymmetric magnetic environment and discussed which modes were likely candidates to be identified and whether thin- or wide-slab applications were more appropriate for each. Naturally, as the asymmetric Cartesian models have kept evolving, these suggestions can and should be reexamined, in the hopes of identifying the model that best fits the given solar structure and captures the most essential pieces of physics driving its dynamic processes.

The global atmospheric applications suggested so far involve the vertical stratification of the atmosphere. It must be noted that the asymmetric model family reviewed here does not take into consideration two important factors that can play a role in large-scale applications: the curvature of the layers in the Sun's atmosphere and the effects of gravity. Therefore, before attempting global applications of these Cartesian models, it must be assumed that the gravitational scale height and the radius of curvature are both much larger than the investigated characteristic length scales. If these conditions are both met, then, as a first approximation, one can think of a slice of the solar atmosphere as a series of horizontal segments separated by plane-parallel layers. One possibility is to consider the lowest and highest atmospheric layers, the photosphere and the corona as the asymmetric environment, and construct a slab in between them out of the so-called interface region, which itself is made up of the chromosphere and the narrow transition region. In order to further

refine this model, it is possible to use a two-slab geometry similar to the one described by Shukhobodskaia and Erdélyi [85]. Alternately, we may turn our attention to the top half of this model and investigate the triad of the chromosphere, the transition region, and the corona as a single-slab model. These applications also tie the asymmetric slab studies to the broader question of solar atmospheric heating, namely the outermost layer of the Sun's atmosphere, the corona, can reach temperatures of millions of degrees, which is three orders of magnitude higher than the temperature at the visible surface of the Sun, which is much closer to our star's internal fusion energy production. Numerous attempts have been made to explain this puzzling observation of the solar coronal and chromospheric heating problem. One possible source of the additional energy required to keep the chromosphere and the corona warmer than the underlying photosphere was found in the form of MHD waves guided by the ubiquitous magnetic fields all throughout the solar atmosphere, turning it into a coupled system (Erdélyi [3], Komm et al. [29]). Alfvén waves continue to be one of the special focus areas of wave-based atmospheric heating mechanisms (see, e.g., Erdélyi and Fedun [116], Liu et al. [117]). As both modelling capabilities improve (see Van Doorsselaere et al. [118]) and the available resolution of our instruments increases (Taroyan and Erdélyi [119], Cargill and de Moortel [120], Jess et al. [121], Stangalini [122]), we reach an ever-clearer picture of how various solar waveguides can contribute to a full understanding of the complex question of atmospheric heating.

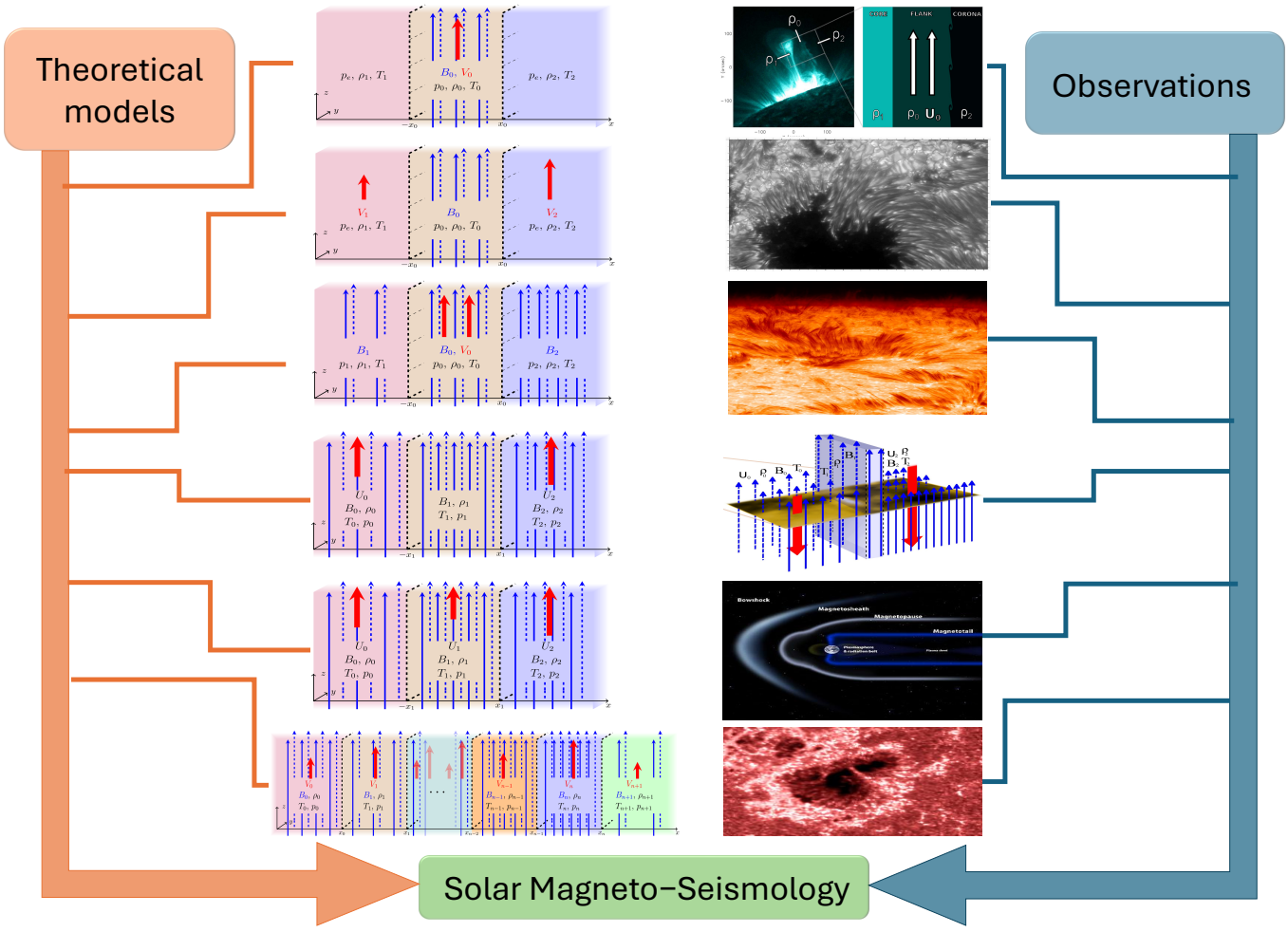

Figure 11. The family of recent steady asymmetric slab models and their potential applications to observable structures in solar magneto-seismology.

There is also a rich variety of intermediate- and small-scale features in the solar atmosphere that yield themselves to local applications of multi-layered asymmetric Cartesian

models. Some of these possibilities were also explored by Barbulescu and Erdélyi [96], Allcock et al. [46], and Zsámberger and Erdélyi [102]. In the upper layers of the solar atmosphere, the boundaries between coronal holes and quiet Sun areas or plumes (DeForest and Gurman [106], Berghmans and Clette [123], Ofman et al. [124], Ofman et al. [125]) could be considered in an asymmetric single-slab system, and an important next step would in this case be the inclusion of bulk background motions in the model.

A further coronal application that has been proposed already by Joarder and Roberts [126] in a symmetric model is that of prominences and their environment, where the detected vertically polarised oscillations have been explained as transverse waves on horizontal magnetic field lines. An early series of studies described oscillations and standing waves considering the possibilities of various boundary and wave vector orientations in a prominence modelled as a magnetic slab system (Joarder and Roberts [126,127,128]). Inspired by these investigations, Oxley et al. [82,83] and Zsámberger and Erdélyi [102] suggested looking at the prominences as asymmetric single-slab systems, as also shown in Figure 12, and investigated the solar magneto-seismological tools that could be developed when searching for standing or propagating waves guided by prominences, respectively. On the observational side, Arregui et al. [103] provides an overview of oscillations of various amplitudes found in prominences, as well as detection methods. Along with Arregui and Ballester [129], the study also discusses the damping of prominence oscillations. How these properties can provide insights into the physical properties of prominences that cannot be derived from direct observation is discussed in, e.g., Banerjee et al. [5] and Oliver [130], providing reviews of prominence seismology.

Finally, as mentioned before, Barbulescu and Erdélyi [96] used the model of a single magnetic slab under the effect of a steady flow, enclosed between two layers of a non-magnetic, asymmetric, static environment, to model the flank region of a CME and make successful deductions about the density ratio between the different layers of this model. The authors suggested that the estimates could be further improved by considering the presence of asymmetric external magnetic fields—which could now serve as a test of the model described by Zsámberger et al. [92].

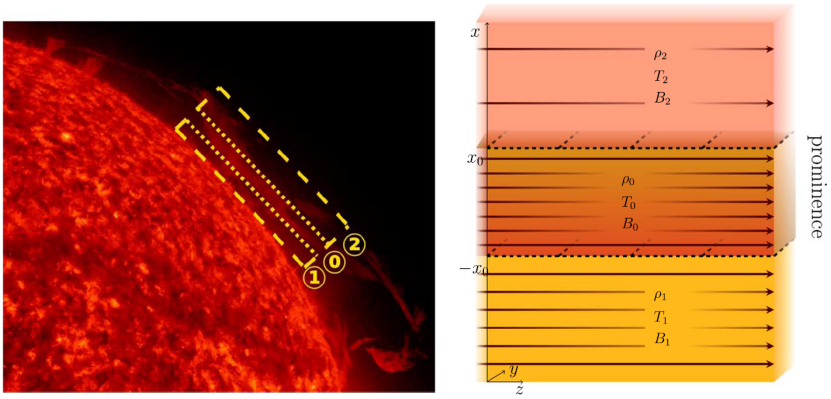

Figure 12. Stratification of the solar atmosphere around a prominence viewed as an asymmetric magnetic slab system incorporating plasma and magnetic asymmetries, but no background flows. The picture on the left shows the orientation of the slab projected over a prominence observation by SDO in the 304 Å channel from 20 July 2013. The right-hand-side image illustrates the necessary rotation of the coordinate system by 90° to adapt the slab model to a prominence above the solar surface. Source: Figure 8 of Zsámberger and Erdélyi [102].

Shifting our focus to the lower layers of the atmosphere, a thorough application of new tools of SMS developed based on the properties of asymmetric eigenmodes was carried out by Allcock and Erdélyi [88], re-examining fibrils in the chromosphere as magnetic slabs embedded in an asymmetric, non-magnetic environment. While Morton et al. [99] interpreted the observed oscillations of the fibrils as concurrent sausage and kink modes in

a magnetic flux tube, Allcock and Erdélyi [88] proposed that they could be interpreted as a manifestation of a single eigenmode in an asymmetric slab waveguide instead, and even provided estimates of the Alfvén speed in the fibril.

Another example of lower atmospheric structures of our Sun that have been interpreted as asymmetric multi-layered (Shukhobodskaia and Erdélyi [85]) or single- (Zsámberger and Erdélyi [102]) slab systems are light bridges, as shown in Figure 13. These are elongated bright areas or bands embedded in the darkest and "coldest" part of sunspots, the umbra, and often, the light bridges can fully split the umbra into two separate cores. Since the two umbral cores they lie between can be entirely separate, they can likely constitute an asymmetric environment, as well. Several oscillating motions have been detected and studied in light bridges and the light walls extending above them; see, e.g., Yuan et al. [131], Yang et al. [132], Hou et al. [133], Yang et al. [134], and Yuan and Walsh [135]. Simulations show the presence of upflows in the central parts of light bridges, and downflows at their lateral edges (Bharti [136]), and so, the changed phase speeds and instability conditions of quasi-sausage and quasi-kink modes guided by light bridges in the presence of asymmetric background flows appear to be a promising area of future study.

Last, but not least, magnetic bright points (MBPs) of the photosphere are also excellent candidates for solar applications of asymmetric Cartesian models. These small concentrations of strong magnetic fields are wedged in dark intergranular lanes formed from the convectional downflow, which separate the cells of the photosphere's granular structure (Rouppe van der Voort et al. [137], Crockett et al. [138], Keys et al. [139]). They are frequently analysed as cylindrical flux tubes; however, they are often strongly elongated, and they can even be quite irregularly shaped, especially near pores [105,140]. While flux tube and slab models are not generally interchangeable, they may help focus on different aspects of a solar atmospheric structure in a first approximation, such as the presence or absence of external asymmetry or flows in this case. A similar argument can be made for light bridges/light walls (see above). Recent studies have also found that, driven by oscillations in the photosphere, spicules can manifest either as flux tube-like jets or sheets of material, the latter of which also lend themselves easily to slab model applications. Additionally, when the available measurements do not strongly obviously reveal the cylindrical/elongated/slab-like structure of a solar atmospheric phenomenon, either approach can be used for modelling and the results compared (see a demonstration of this process in Allcock et al. [46]).

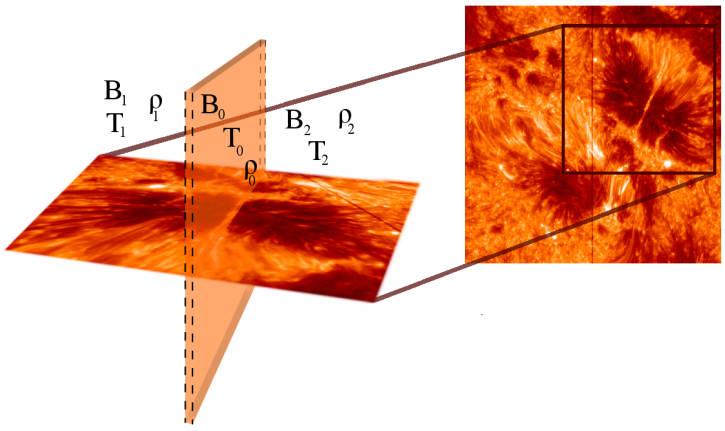

Figure 13. A light bridge viewed as a magnetic slab system incorporating external plasma and magnetic asymmetries, superimposed on a slit-jaw image taken by the Interface Region Imaging Spectrograph (IRIS) in 1400 Å, on 3 July 2014. Source: Figure 10 of Zsámberger and Erdélyi [102].

In the case of MBPs, the above-mentioned heterogeneity in their shapes makes it possible to approach at least some of them as magnetic slabs. Since MBPs are sitting in between two different neighbouring cells of the solar granulation, physical parameters

on either side of a bright point may also show differences. This second fact serves as an excellent motivation to apply specifically asymmetric slab models when studying waves in magnetic bright points. Figure 14 illustrates such an interpretation of an MBP, with the bright region in the centre being the magnetic slab itself, and the intergranular lane it cuts into two halves serving as the asymmetric environment.

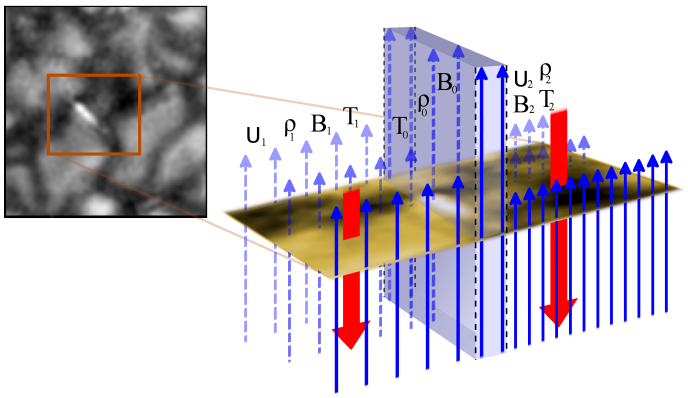

Figure 14. An elongated magnetic bright point viewed as a non-stationary asymmetric slab, where plasma parameters, magnetic field strengths, and flow speeds present in the external regions may all be simultaneously asymmetric (adapted from Figure 12 of Allcock et al. [46]).

As the constantly evolving family of multi-layered Cartesian models kept incorporating additional sources of asymmetry in its slab systems, the applicability of these geometries to MBPs and the expected results were re-examined multiple times, which in itself serves as a powerful illustration of the importance of the model choice itself, and the unique nature of the contributions to the behaviour of the guided waves from each different source of asymmetry. For example, Zsámberger et al. [89], in the first study of a static magnetic slab model incorporating both plasma and magnetic asymmetries, employed the approximation of an incompressible plasma when suggesting the application of the model to MBPs. In this approximation, it was found that only a pair of surface modes could be expected to be present as trapped modes in an MBP slab. Later, Zsámberger and Erdélyi [102] presented an application of the same static asymmetric magnetic slab model in a more generalised case, when two high-β segments of an intergranular lane surround the MBP, which itself could have any value of the plasma-β parameter. In this static case, the choice of internal plasma-β in the system did not change the types of supported solutions fundamentally, as they remained a single pair of surface modes propagating at various speeds and with different cut-off frequencies depending on the speed ordering.

Introducing bulk background flows into the model leads to very different results. Zsámberger et al. [98] found that, even with a relatively weak pair of external flow speeds chosen ($U_1 = -1.2$ km/s and $U_2 = 4.2$ km/s, within the range of estimated downflow speeds near small magnetic elements [1 km/s–10 km/s]; see Briand and Solanki [141], Socas-Navarro et al. [142], and Danilovic et al. [143]), instabilities can be present in the system, as shown in Figure 15a. Additionally, the phase speeds of all solutions are shifted backwards by the downflows, which could even lead to the appearance of body modes in addition to the previously suggested surface waves. While this study already incorporated asymmetric downflows in the intergranular lanes, they were still considered entirely free of magnetic fields, which may not necessarily be the case. Allcock et al. [46], however, contains an example where the intergranular lanes are treated as layers of an asymmetric and magnetic environment. The results given by applying such a model are shown in Figure 15b. With this model and parameter choice (representative of the photosphere), both body mode solutions, and stable, as well as unstable surface mode solutions were found, with a different phase speed shift compared to Figure 15a. It should be noted again that, in a steady slab, the cut-off frequencies of trapped solutions are also shifted by the flow

speeds in both the externally magnetic and non-magnetic models. However, the inclusion of external asymmetric magnetic fields results in additional forbidden regions between the Doppler-shifted Alfvén and tube speeds, in which the waves would become leaky. In both cases, instabilities could only be found in thin slabs for the selected external flow speeds, although the extent of this range itself in the dimensionless slab width parameter varies a little between the two models. As the slab considered becomes wider compared to the wavelength of the studied oscillations, the solutions can remain stable. Similar to what was discussed earlier in relation to Figure 9, the instability can still exist for the relatively low, sub-Alfvénic external flow speeds chosen here due to the presence of the flow asymmetry. A future direction of improving upon modelling MBPs could be investigating how these instability conditions change when further details of the surrounding photosphere are also taken into consideration. Based on the application of a multi-slab model such as the one described at the beginning of Section 3, or by Shukhobodskaia and Erdélyi [85] and Allcock et al. [46], it becomes possible to also include information on the granular cells themselves separated by the region of the dark intergranular lane containing the MBP.

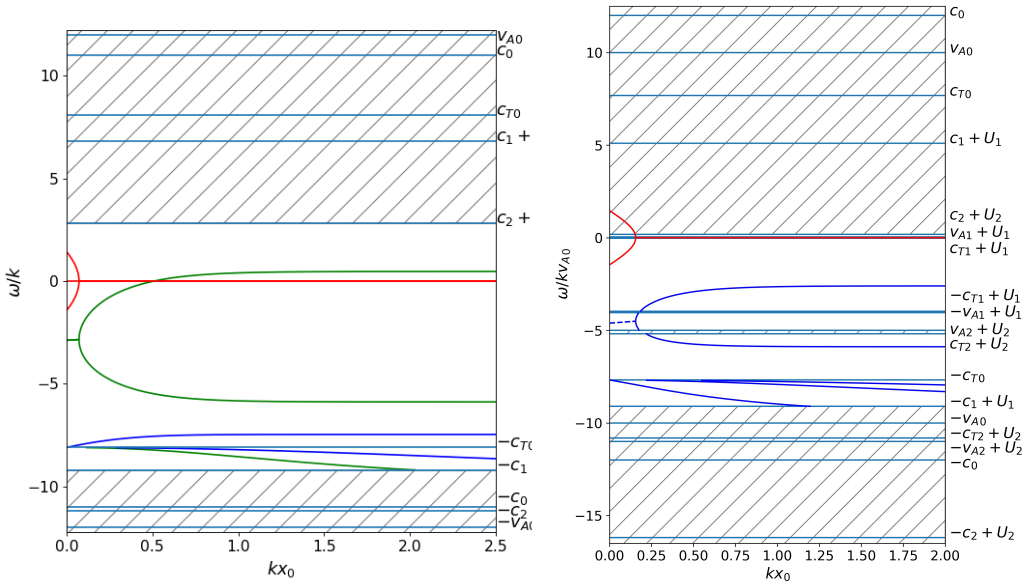

(**a**) (**b**)

Figure 15. (**a**) Solutions to the dispersion relation in (**a**) an externally non-magnetic slab system incorporating density and flow asymmetries, adapted from Figure 2 of Zsámberger et al. [98] and (**b**) an asymmetric magnetic slab with external flow asymmetry, adapted from Figure 13 of Allcock et al. [46].

5. Conclusions

The previous sections have provided a brief review of recent advances made in uncovering the role that symmetry and asymmetry play in the propagation of MHD waves, focused on a solar environment and possible applications in the field of SMS. We have presented the composition, advantages, and key results of several, asymmetric and symmetric magnetic slab models applicable to different structures within the solar atmosphere, including models of a single slab and its environment, as well as the most generalised version of a multi-layered Cartesian waveguide incorporating plasma, magnetic, and flow asymmetries. We explained the main features of quasi-sausage and quasi-kink eigenmodes in an asymmetric waveguide, which could then be utilised in crafting and applying tools of solar magneto-seismology to various different atmospheric structures. While in some cases, new analyses of existing data are possible, when it comes to applications, especially for small-scale lower atmospheric features, the applications of such tools will become possible only with the higher spatial and temporal resolution measurements of next-generation solar telescopes such as DKIST.

We took great care in identifying the additional physics incorporated into every gradually built new model and outlining which source of asymmetry (or lack thereof) is responsible for which new, potentially unexpected facet of MHD wave propagation that the analytical and numerical modelling efforts uncovered. It should be noted that, however useful layered asymmetric waveguides are as proxies for inhomogeneities in physical parameters of the solar atmosphere, the results provided by their application must not be overinterpreted. Depending on the nature and type of the solar structure under investigation, and the specific aspect of it under study, carefully weighed choices must be made between cylindrical and Cartesian models. Further refinements of these specific models, e.g., including non-linear effects, or incorporating gradients instead of sharp discontinuities may both help capture an additional aspect of MHD wave behaviour in the solar plasma, but they may also sacrifice some of the analytical tractability.

In Section 4, we demonstrated that the choice of the model has a significant influence on what aspect of a certain solar waveguide we are able to study. This is true both for picking which sources of asymmetry to incorporate, as well as for deciding between flux tube or slab models. Some features of the solar atmosphere may yield themselves to both geometries, depending on the available information (see, e.g., the multiple studies of chromospheric fibrils as slabs (Morton et al. [99], Allcock et al. [46]) or the variety in the shapes of MBPs). For a more complex understanding of asymmetric solar MHD waveguide models, additional effects such as propagation not only in the z- but also in the y-direction or gravitational stratification may be brought back into consideration. Various alternate sources of instabilities can be considered as well, such as investigating the effects of different velocity profiles on the KHI threshold in either slabs or cylinders (see some early kick-off works by, e.g., Michalke [144], Blumen [145], Ray [146], Wu and Wang [147]).

Overall, while there is always room for introducing more meaningful physical complexity into our waveguide models, exploring the influence of breaking the symmetry in the classical building blocks of modelling the solar atmosphere has provided us with new insight into MHD wave propagation and waveguide stability, and it also led to the development of new diagnostic tools for SMS purposes. As demonstrated, several applications can be found for the asymmetric model family in the dynamic solar atmosphere, allowing us to gain valuable information on the workings of our star, as long as we keep both the strengths and the limitations of our modelling efforts in mind.

Funding: R.E. acknowledges support from the European Union's Horizon 2020 research and innovation programme under grant agreement No. 739500 (PRE-EST project) and No. 824135 (SOLARNET project). R.E. also thanks the support received from NKFIH OTKA (Hungary, grant No. K142987) and from ISSI-BJ ("Step forward in solar flare and coronal mass ejection (CME) predicting"). R.E. is grateful to STFC (U.K., grant number ST/M000826/1) and PIFI of the Chinese Academy of Sciences (grant No. 2024PVA0043). This work was also supported by the NKFIH Excellence Grant TKP2021-NKTA-64. N.K.Z. and R.E. are further thankful for the support received from STFC (U.K.) under grant number ST/V003712/1.

Acknowledgments: The authors are grateful to the University of Sheffield for its long-standing support of the research into the topic of this review. We would further like to thank M. Barbulescu for making the PyTES software package available (https://github.com/BarbulescuMihai/PyTES (accessed on 24 September 2018)), which was used as the basis of solvers in a number of the referenced publications on asymmetric slabs to obtain solutions to the various models' dispersion relations.

Conflicts of Interest: The authors declare no conflict of interest.

References

1. Rast, M.P.; Bello González, N.; Bellot Rubio, L.; Cao, W.; Cauzzi, G.; Deluca, E.; de Pontieu, B.; Fletcher, L.; Gibson, S.E.; Judge, P.G.; et al. Critical Science Plan for the Daniel K. Inouye Solar Telescope (DKIST). *Sol. Phys.* **2021**, *296*, 70. [CrossRef]
2. Quintero Noda, C.; Schlichenmaier, R.; Bellot Rubio, L.R.; Löfdahl, M.G.; Khomenko, E.; Jurčák, J.; Leenaarts, J.; Kuckein, C.; González Manrique, S.J.; Gunár, S.; et al. The European Solar Telescope. *Astron. Astrophys.* **2022**, *666*, A21. [CrossRef]
3. Erdélyi, R. Magnetic coupling of waves and oscillations in the lower solar atmosphere: Can the tail wag the dog? *Philos. Trans. R. Soc. Lond. Ser. A* **2006**, *364*, 351–381. [CrossRef] [PubMed]

4. Erdélyi, R. Magnetic seismology of the lower solar atmosphere. In Proceedings of the SOHO 18/GONG 2006/HELAS I, Beyond the Spherical Sun, Sheffield, UK, 7–11 August 2006; ESA Special Publication: Noordwijk, The Netherlands 2006; Volume 624, p. 15.1.
5. Banerjee, D.; Erdélyi, R.; Oliver, R.; O'Shea, E. Present and Future Observing Trends in Atmospheric Magnetoseismology. *Sol. Phys.* **2007**, *246*, 3–29. [CrossRef]
6. Nakariakov, V.M.; Pilipenko, V.; Heilig, B.; Jelínek, P.; Karlický, M.; Klimushkin, D.Y.; Kolotkov, D.Y.; Lee, D.H.; Nisticò, G.; Van Doorsselaere, T.; et al. Magnetohydrodynamic Oscillations in the Solar Corona and Earth's Magnetosphere: Towards Consolidated Understanding. *Space Sci. Rev.* **2016**, *200*, 75–203. [CrossRef]
7. Jess, D.B.; Jafarzadeh, S.; Keys, P.H.; Stangalini, M.; Verth, G.; Grant, S.D.T. Waves in the lower solar atmosphere: The dawn of next-generation solar telescopes. *Living Rev. Sol. Phys.* **2023**, *20*, 1. [CrossRef]
8. Leighton, R.B.; Noyes, R.W.; Simon, G.W. Velocity Fields in the Solar Atmosphere. I. Preliminary Report. *Astrophys. J.* **1962**, *135*, 474. [CrossRef]
9. Ulrich, R.K. The Five-Minute Oscillations on the Solar Surface. *Astrophys. J.* **1970**, *162*, 993. [CrossRef]
10. Leibacher, J.W.; Stein, R.F. A New Description of the Solar Five-Minute Oscillation. *Astrophys. J. Lett.* **1971**, *7*, 191–192.
11. Roberts, B.; Edwin, P.M.; Benz, A.O. On coronal oscillations. *Astrophys. J.* **1984**, *279*, 857–865. [CrossRef]
12. Nakariakov, V.M.; Ofman, L. Determination of the coronal magnetic field by coronal loop oscillations. *Astron. Astrophys.* **2001**, *372*, L53–L56. [CrossRef]
13. Wang, T.; Innes, D.E.; Qiu, J. Determination of the Coronal Magnetic Field from Hot-Loop Oscillations Observed by SUMER and SXT. *Astrophys. J.* **2007**, *656*, 598–609. [CrossRef]
14. Erdélyi, R.; Taroyan, Y. Hinode EUV spectroscopic observations of coronal oscillations. *Astron. Astrophys.* **2008**, *489*, L49–L52. [CrossRef]
15. Andries, J.; Arregui, I.; Goossens, M. Determination of the Coronal Density Stratification from the Observation of Harmonic Coronal Loop Oscillations. *Astrophys. J. Lett.* **2005**, *624*, L57–L60. [CrossRef]
16. Van Doorsselaere, T.; Wardle, N.; Del Zanna, G.; Jansari, K.; Verwichte, E.; Nakariakov, V.M. The First Measurement of the Adiabatic Index in the Solar Corona Using Time-dependent Spectroscopy of Hinode/EIS Observations. *Astrophys. J. Lett.* **2011**, *727*, L32. [CrossRef]
17. Nakariakov, V.M.; Verwichte, E. Coronal Waves and Oscillations. *Living Rev. Sol. Phys.* **2005**, *2*, 3. [CrossRef]
18. De Moortel, I.; Nakariakov, V.M. Magnetohydrodynamic waves and coronal seismology: An overview of recent results. *Philos. Trans. R. Soc. Lond. Ser. A* **2012**, *370*, 3193–3216. [CrossRef]
19. Andries, J.; van Doorsselaere, T.; Roberts, B.; Verth, G.; Verwichte, E.; Erdélyi, R. Coronal Seismology by Means of Kink Oscillation Overtones. *Space Sci. Rev.* **2009**, *149*, 3–29. [CrossRef]
20. Ruderman, M.S.; Erdélyi, R. Transverse Oscillations of Coronal Loops. *Space Sci. Rev.* **2009**, *149*, 199–228. [CrossRef]
21. Guo, Y.; Erdélyi, R.; Srivastava, A.K.; Hao, Q.; Cheng, X.; Chen, P.F.; Ding, M.D.; Dwivedi, B.N. Magnetohydrodynamic Seismology of a Coronal Loop System by the First Two Modes of Standing Kink Waves. *Astrophys. J.* **2015**, *799*, 151. [CrossRef]
22. Chen, G.Y.; Guo, Y.; Ding, M.D.; Erdélyi, R. Measuring local physical parameters in coronal loops with spatial seismology. *Astron. Astrophys.* **2023**, *678*, A205. [CrossRef]
23. Beckers, J.M. Solar Spicules. *Annu. Rev. Astron. Astrophys.* **1972**, *10*, 73. [CrossRef]
24. Sterling, A.C. Solar Spicules: A Review of Recent Models and Targets for Future Observations—(Invited Review). *Sol. Phys.* **2000**, *196*, 79–111. [CrossRef]
25. De Pontieu, B.; Erdélyi, R.; James, S.P. Solar chromospheric spicules from the leakage of photospheric oscillations and flows. *Nature* **2004**, *430*, 536–539. [CrossRef] [PubMed]
26. Pereira, T.M.D.; De Pontieu, B.; Carlsson, M. Quantifying Spicules. *Astrophys. J.* **2012**, *759*, 18, [CrossRef]
27. Martínez-Sykora, J.; De Pontieu, B.; Hansteen, V.H.; Rouppe van der Voort, L.; Carlsson, M.; Pereira, T.M.D. On the generation of solar spicules and Alfvénic waves. *Science* **2017**, *356*, 1269–1272. [CrossRef]
28. Zaqarashvili, T.V.; Erdélyi, R. Oscillations and Waves in Solar Spicules. *Space Sci. Rev.* **2009**, *149*, 355–388. [CrossRef]
29. Komm, R.; De Moortel, I.; Fan, Y.; Ilonidis, S.; Steiner, O. Sub-photosphere to Solar Atmosphere Connection. *Space Sci. Rev.* **2015**, *196*, 167–199. [CrossRef]
30. Berger, T.E.; Slater, G.; Hurlburt, N.; Shine, R.; Tarbell, T.; Title, A.; Lites, B.W.; Okamoto, T.J.; Ichimoto, K.; Katsukawa, Y.; et al. Quiescent Prominence Dynamics Observed with the Hinode Solar Optical Telescope. I. Turbulent Upflow Plumes. *Astrophys. J.* **2010**, *716*, 1288–1307. [CrossRef]
31. Ryutova, M.; Berger, T.; Frank, Z.; Tarbell, T.; Title, A. Observation of Plasma Instabilities in Quiescent Prominences. *Sol. Phys.* **2010**, *267*, 75–94. [CrossRef]
32. Skirvin, S.J.; Fedun, V.; Verth, G.I. The effect of symmetric and spatially varying equilibria and flow on MHD wave modes: Slab geometry. *Mon. Not. Roy. Astron. Soc.* **2021**, *504*, 4077–4092. [CrossRef]
33. Yu, H.; Li, B.; Chen, S.; Guo, M. Resonant Damping of Kink Modes in Solar Coronal Slabs. *Sol. Phys.* **2021**, *296*, 95. [CrossRef]
34. Chen, S.X.; Li, B.; Guo, M.; Shi, M.; Yu, H. Oblique Quasi-kink Modes in Solar Coronal Slabs Embedded in an Asymmetric Magnetic Environment: Resonant Damping, Phase and Group Diagrams. *Astrophys. J.* **2022**, *940*, 157. [CrossRef]
35. Shi, M.; Li, B.; Yuan, S. Horizontally Polarized Kink Oscillations Supported by Solar Coronal Loops in an Asymmetric Environment. *arXiv* **2024**. [CrossRef]

36. Tirry, W.J.; Cadez, V.M.; Erdelyi, R.; Goossens, M. Resonant flow instability of MHD surface waves. *Astron. Astrophys.* **1998**, *332*, 786–794.
37. Walker, A.D.M. Reflection and transmission at the boundary between two counterstreaming MHD plasmas—Active boundaries or negative-energy waves? *J. Plasma Phys.* **2000**, *63*, 203–219. [CrossRef]
38. Taroyan, Y.; Erdélyi, R. Resonant and Kelvin–Helmholtz instabilities on the magnetopause. *Phys. Plasmas* **2002**, *9*, 3121–3129. [CrossRef]
39. Erkaev, N.V.; Semenov, V.S.; Biernat, H.K. Magnetic Double-Gradient Instability and Flapping Waves in a Current Sheet. *Phys. Rev. Lett.* **2007**, *99*, 235003. [CrossRef]
40. Korovinskiy, D.B.; Divin, A.; Erkaev, N.V.; Ivanova, V.V.; Ivanov, I.B.; Semenov, V.S.; Lapenta, G.; Markidis, S.; Biernat, H.K.; Zellinger, M. MHD modeling of the double-gradient (kink) magnetic instability. *J. Geophys. Res. (Space Phys.)* **2013**, *118*, 1146–1158. [CrossRef]
41. Zelenyi, L.; Artemyev, A.; Petrukovich, A. Properties of Magnetic Field Fluctuations in the Earth's Magnetotail and Implications for the General Problem of Structure Formation in Hot Plasmas. *Space Sci. Rev.* **2015**, *188*, 287–310. [CrossRef]
42. Zaqarashvili, T.V.; Lomineishvili, S.; Leitner, P.; Hanslmeier, A.; Gömöry, P.; Roth, M. Kink instability of triangular jets in the solar atmosphere. *Astron. Astrophys.* **2021**, *649*, A179. [CrossRef]
43. Aschwanden, M.J.; Fletcher, L.; Schrijver, C.J.; Alexander, D. Coronal Loop Oscillations Observed with the Transition Region and Coronal Explorer. *Astrophys. J.* **1999**, *520*, 880–894. [CrossRef]
44. Nakariakov, V.M.; Ofman, L.; Deluca, E.E.; Roberts, B.; Davila, J.M. TRACE observation of damped coronal loop oscillations: Implications for coronal heating. *Science* **1999**, *285*, 862–864. [CrossRef] [PubMed]
45. Van Doorsselaere, T.; Nakariakov, V.M.; Young, P.R.; Verwichte, E. Coronal magnetic field measurement using loop oscillations observed by Hinode/EIS. *Astron. Astrophys.* **2008**, *487*, L17–L20. [CrossRef]
46. Allcock, M.; Shukhobodskaia, D.; Zsámberger, N.K.; Erdélyi, R. Magnetohydrodynamic waves in multi-layered asymmetric waveguides: Solar magneto-seismology theory and application. *Front. Astron. Space Sci.* **2019**, *6*, 48. [CrossRef]
47. Roberts, B. Wave Propagation in a Magnetically Structured Atmosphere—Part One—Surface Waves at a Magnetic Interface. *Sol. Phys.* **1981**, *69*, 27–38. [CrossRef]
48. Roberts, B. Wave Propagation in a Magnetically Structured Atmosphere—Part Two—Waves in a Magnetic Slab. *Sol. Phys.* **1981**, *69*, 39–56. [CrossRef]
49. Edwin, P.M.; Roberts, B. Wave Propagation in a Magnetically Structured Atmosphere—Part Three—The Slab in a Magnetic Environment. *Sol. Phys.* **1982**, *76*, 239–259. [CrossRef]
50. Ruderman, M.S. Soliton propagation on multiple-interface magnetic structures. *J. Geophys. Res.* **1992**, *97*, 16. [CrossRef]
51. Díaz, A.J.; Oliver, R.; Ballester, J.L. Fast magnetohydrodynamic oscillations in a multifibril Cartesian prominence model. *Astron. Astrophys.* **2005**, *440*, 1167–1175. [CrossRef]
52. Díaz, A.J.; Roberts, B. Fast Magnetohydrodynamic Oscillations in a Fibril Prominence Model. *Sol. Phys.* **2006**, *236*, 111–126. [CrossRef]
53. Luna, M.; Terradas, J.; Oliver, R.; Ballester, J.L. Fast magnetohydrodynamic waves in a two-slab coronal structure: Collective behaviour. *Astron. Astrophys.* **2006**, *457*, 1071–1079. [CrossRef]
54. De Pontieu, B.; McIntosh, S.; Hansteen, V.H.; Carlsson, M.; Schrijver, C.J.; Tarbell, T.D.; Title, A.M.; Shine, R.A.; Suematsu, Y.; Tsuneta, S.; et al. A Tale of Two Spicules: The Impact of Spicules on the Magnetic Chromosphere. *Pub. Astron. Soc. Jpn.* **2007**, *59*, S655. [CrossRef]
55. Pike, C.D.; Mason, H.E. Rotating Transition Region Features Observed with the SOHO Coronal Diagnostic Spectrometer. *Sol. Phys.* **1998**, *182*, 333–348. [CrossRef]
56. Shibata, K.; Ishido, Y.; Acton, L.W.; Strong, K.T.; Hirayama, T.; Uchida, Y.; McAllister, A.H.; Matsumoto, R.; Tsuneta, S.; Shimizu, T.; et al. Observations of X-Ray Jets with the YOHKOH Soft X-Ray Telescope. *Pub. Astron. Soc. Jpn.* **1992**, *44*, L173–L179. [CrossRef]
57. Nakariakov, V.M.; Roberts, B. Magnetosonic Waves in Structured Atmospheres with Steady Flows, I. *Sol. Phys.* **1995**, *159*, 213–228. [CrossRef]
58. Parker, E.N. The Nature of the Sunspot Phenomenon. II: Internal Overstable Modes. *Sol. Phys.* **1974**, *37*, 127–144. [CrossRef]
59. Defouw, R.J. Wave propagation along a magnetic tube. *Astrophys. J.* **1976**, *209*, 266–269. [CrossRef]
60. Ryutov, D.A.; Ryutova, M.P. Sound oscillations in a plasma with "magnetic filaments". *Sov. J. Exp. Theor. Phys.* **1976**, *43*, 491.
61. Roberts, B.; Webb, A.R. Vertical motions in an intense magnetic flux tube. *Sol. Phys.* **1978**, *56*, 5–35. [CrossRef]
62. Wentzel, D.G. On the role of hydrodynamic waves in the corona and the base of the solar wind. *Sol. Phys.* **1977**, *52*, 163–177. [CrossRef]
63. Wentzel, D.G. Hydromagnetic surface waves. *Astrophys. J.* **1979**, *227*, 319–322. [CrossRef]
64. Zaitsev, V.V.; Stepanov, A.V.; Sterlin, A.M. The Microwave Pulsations in Solar Flares—Magnetohydrodynamic and Plasma Models. *Sov. Astron. Lett.* **1985**, *11*, 192–194.
65. Spruit, H.C.; Roberts, B. Magnetic flux tubes on the Sun. *Nature* **1983**, *304*, 401–406. [CrossRef]
66. Edwin, P.M.; Roberts, B. Wave Propagation in a Magnetic Cylinder. *Sol. Phys.* **1983**, *88*, 179–191. [CrossRef]
67. Gu, Y.N.; Qiu, N.X. Kink instabilities of a plasma column with elliptical cross-section. *Acta Phys. Sin.* **1980**, *29*, 1367–1377.

68. Ruderman, M.S. The resonant damping of oscillations of coronal loops with elliptic cross-sections. *Astron. Astrophys.* **2003**, *409*, 287–297. [CrossRef]
69. Erdélyi, R.; Morton, R.J. Magnetohydrodynamic waves in a compressible magnetic flux tube with elliptical cross-section. *Astron. Astrophys.* **2009**, *494*, 295–309. [CrossRef]
70. Morton, R.J.; Ruderman, M.S. Kink and fluting modes of stratified coronal magnetic loops with elliptical cross-sections. *Astron. Astrophys.* **2011**, *527*, A53. [CrossRef]
71. Aldhafeeri, A.A.; Verth, G.; Brevis, W.; Jess, D.B.; McMurdo, M.; Fedun, V. Magnetohydrodynamic Wave Modes of Solar Magnetic Flux Tubes with an Elliptical Cross Section. *Astrophys. J.* **2021**, *912*, 50. [CrossRef]
72. Mikhalyaev, B.B.; Solov'ev, A.A. MHD Waves in Coronal Loops with a Shell. *Astron. Lett.* **2004**, *30*, 268–275. [CrossRef]
73. Mikhalyaev, B.B.; Solov'ev, A.A. The Oscillations of Coronal Loops Including the Shell. *Sol. Phys.* **2005**, *227*, 249–263. [CrossRef]
74. Carter, B.K.; Erdélyi, R. Sausage and kink oscillations in incompressible annular magnetic cylinders. *Astron. Astrophys.* **2007**, *475*, 323–331. [CrossRef]
75. Carter, B.K.; Erdélyi, R. Kink oscillations in magnetic tubes with twisted annulus. *Astron. Astrophys.* **2008**, *481*, 239–246. [CrossRef]
76. Lopin, I. Kink oscillations in a coronal loop arcade with finite plasma-β: Effect of oblique propagation. *Mon. Not. Roy. Astron. Soc.* **2022**, *514*, 4329–4342. [CrossRef]
77. Dover, F.M.; Sharma, R.; Korsós, M.B.; Erdélyi, R. Signatures of Cross-sectional Width Modulation in Solar Spicules due to Field-aligned Flows. *Astrophys. J.* **2020**, *905*, 72. [CrossRef]
78. Mackenzie Dover, F.; Sharma, R.; Erdélyi, R. Magnetohydrodynamic Simulations of Spicular Jet Propagation Applied to Lower Solar Atmosphere Model. II. Case Studies with Tilted Jets. *Astrophys. J.* **2022**, *929*, 88. [CrossRef]
79. Skirvin, S.J.; Gao, Y.; Van Doorsselaere, T. Alfvénic Motions Arising from Asymmetric Acoustic Wave Drivers in Solar Magnetic Structures. *Astrophys. J.* **2023**, *949*, 38. [CrossRef]
80. Mather, J.F.; Erdélyi, R. Magneto-Acoustic Waves in a Gravitationally Stratified Magnetized Plasma: Eigen-Solutions and their Applications to the Solar Atmosphere. *Astrophys. J.* **2016**, *822*, 116. [CrossRef]
81. Lopin, I.; Nagorny, I. Kink Waves in Non-isothermal Stratified Solar Waveguides: Effect of the External Magnetic Field. *Astron. J.* **2017**, *154*, 141. [CrossRef]
82. Oxley, W.; Zsámberger, N.K.; Erdélyi, R. Standing MHD Waves in a Magnetic Slab Embedded in an Asymmetric Plasma Environment: Slow Surface Waves. *Astrophys. J.* **2020**, *890*, 109. [CrossRef]
83. Oxley, W.; Zsámberger, N.K.; Erdélyi, R. Standing MHD Waves in a Magnetic Slab Embedded in an Asymmetric Magnetic Plasma Environment: Surface Waves. *Astrophys. J.* **2020**, *898*, 19. [CrossRef]
84. Allcock, M.; Erdélyi, R. Magnetohydrodynamic Waves in an Asymmetric Magnetic Slab. *Sol. Phys.* **2017**, *292*, 35. [CrossRef] [PubMed]
85. Shukhobodskaia, D.; Erdélyi, R. Propagation of Surface Magnetohydrodynamic Waves in Asymmetric Multilayered Plasma. *Astrophys. J.* **2018**, *868*, 128. [CrossRef]
86. Lopin, I.; Nagorny, I. Oscillations of a coronal plasma slab excited by an external source. *Mon. Not. Roy. Astron. Soc.* **2020**, *496*, 3035–3042. [CrossRef]
87. Li, B.; Antolin, P.; Guo, M.Z.; Kuznetsov, A.A.; Pascoe, D.J.; Van Doorsselaere, T.; Vasheghani Farahani, S. Magnetohydrodynamic Fast Sausage Waves in the Solar Corona. *Space Sci. Rev.* **2020**, *216*, 136. [CrossRef]
88. Allcock, M.; Erdélyi, R. Solar Magnetoseismology with Magnetoacoustic Surface Waves in Asymmetric Magnetic Slab Waveguides. *Astrophys. J.* **2018**, *855*, 90. [CrossRef]
89. Zsámberger, N.K.; Allcock, M.; Erdélyi, R. Magneto-acoustic Waves in a Magnetic Slab Embedded in an Asymmetric Magnetic Environment: The Effects of Asymmetry. *Astrophys. J.* **2018**, *853*, 136. [CrossRef]
90. Zsámberger, N.K.; Erdélyi, R. Solar Magneto-seismology of a Magnetic Slab in an Asymmetric Magnetic Environment. *Astrophys. J.* **2022**, *934*, 155. [CrossRef]
91. Allcock, M.M. Asymmetric Magnetohydrodynamic Waves of the Solar Atmosphere. Ph.D. Dissertation, University of Sheffield, Sheffield, UK, 2020.
92. Zsámberger, N.K.; Tong, Y.; Asztalos, B.; Erdélyi, R. MHD Wave Propagation and the Kelvin–Helmholtz Instability in an Asymmetric Magnetic Slab System. *Astrophys. J.* **2022**, *935*, 41. [CrossRef]
93. Zsámberger, N.K.; Erdélyi, R. Magnetoacoustic Waves in a Magnetic Slab Embedded in an Asymmetric Magnetic Environment. II. Thin and Wide Slabs, Hot and Cold Plasmas. *Astrophys. J.* **2020**, *894*, 123. [CrossRef]
94. Taroyan, Y.; Ruderman, M.S. MHD Waves and Instabilities in Space Plasma Flows. *Space Sci. Rev.* **2011**, *158*, 505–523. [CrossRef]
95. Ryutova, M. *Physics of Magnetic Flux Tubes*; Astrophysics and Space Science Library, Springer: Berlin/Heidelberg, Germany, 2015; Volume 417. [CrossRef]
96. Barbulescu, M.; Erdélyi, R. Magnetoacoustic Waves and the Kelvin–Helmholtz Instability in a Steady Asymmetric Slab. I: The Effects of Varying Density Ratios. *Sol. Phys.* **2018**, *293*, 86. [CrossRef] [PubMed]
97. Foullon, C.; Verwichte, E.; Nykyri, K.; Aschwanden, M.J.; Hannah, I.G. Kelvin–Helmholtz Instability of the CME Reconnection Outflow Layer in the Low Corona. *Astrophys. J.* **2013**, *767*, 170. [CrossRef]
98. Zsámberger, N.K.; Sánchez Montoya, C.M.; Erdélyi, R. Magnetohydrodynamic Waves in an Asymmetric Magnetic Slab with Different External Flows. *Astrophys. J.* **2022**, *937*, 23. [CrossRef]

99. Morton, R.J.; Verth, G.; Jess, D.B.; Kuridze, D.; Ruderman, M.S.; Mathioudakis, M.; Erdélyi, R. Observations of ubiquitous compressive waves in the Sun's chromosphere. *Nat. Commun.* **2012**, *3*, 1315. [CrossRef]
100. Mooroogen, K.; Morton, R.J.; Henriques, V. Dynamics of internetwork chromospheric fibrils: Basic properties and magnetohydrodynamic kink waves. *Astron. Astrophys.* **2017**, *607*, A46. [CrossRef]
101. Priest, E. *Magnetohydrodynamics of the Sun*; Cambridge University Press: Cambridge, UK, 2014. [CrossRef]
102. Zsámberger, N.K.; Erdélyi, R. Magnetoacoustic Waves in a Magnetic Slab Embedded in an Asymmetric Magnetic Environment. III. Applications to the Solar Atmosphere. *Astrophys. J.* **2021**, *906*, 122. [CrossRef]
103. Arregui, I.; Oliver, R.; Ballester, J.L. Prominence Oscillations. *Living Rev. Sol. Phys.* **2012**, *9*, 2. [CrossRef]
104. Abramenko, V.; Yurchyshyn, V.; Goode, P.; Kilcik, A. Statistical Distribution of Size and Lifetime of Bright Points Observed with the New Solar Telescope. *Astrophys. J. Lett.* **2010**, *725*, L101–L105. [CrossRef]
105. Bovelet, B.; Wiehr, E. Dynamics of the solar active region finestructure. *Astron. Astrophys.* **2003**, *412*, 249–255. [CrossRef]
106. DeForest, C.E.; Gurman, J.B. Observation of Quasi-periodic Compressive Waves in Solar Polar Plumes . *Astrophys. J. Lett.* **1998**, *501*, L217–L220. [CrossRef]
107. Poletto, G. Solar Coronal Plumes. *Living Rev. Sol. Phys.* **2015**, *12*, 7. [CrossRef]
108. Vazquez, M. A Morphological Study of the Light-Bridges in Sunspots. *Sol. Phys.* **1973**, *31*, 377–387. [CrossRef]
109. Sobotka, M.; Švanda, M.; Jurčák, J.; Heinzel, P.; Del Moro, D.; Berrilli, F. Dynamics of the solar atmosphere above a pore with a light bridge. *Astron. Astrophys.* **2013**, *560*, A84. [CrossRef]
110. Lagg, A.; Solanki, S.K.; van Noort, M.; Danilovic, S. Vigorous convection in a sunspot granular light bridge. *Astron. Astrophys.* **2014**, *568*, A60. [CrossRef]
111. Foullon, C.; Verwichte, E.; Nakariakov, V.M.; Nykyri, K.; Farrugia, C.J. Magnetic Kelvin–Helmholtz Instability at the Sun. *Astrophys. J. Lett.* **2011**, *729*, L8. [CrossRef]
112. Tsiropoula, G. Physical parameters and flows along chromospheric penumbral fibrils. *Astron. Astrophys.* **2000**, *357*, 735–742.
113. Borrero, J.M.; Ichimoto, K. Magnetic Structure of Sunspots. *Living Rev. Sol. Phys.* **2011**, *8*, 4. [CrossRef]
114. Turkakin, H.; Rankin, R.; Mann, I.R. Primary and secondary compressible Kelvin–Helmholtz surface wave instabilities on the Earth's magnetopause. *J. Geophys. Res. Space Phys.* **2013**, *118*, 4161–4175. [CrossRef]
115. Nenovski, P. MHD surface waves—A source of global magnetospheric modes (resonances)? *Adv. Space Res.* **2021**, *67*, 731–738. [CrossRef]
116. Erdélyi, R.; Fedun, V. Are There Alfvén Waves in the Solar Atmosphere? *Science* **2007**, *318*, 1572. [CrossRef] [PubMed]
117. Liu, J.; Nelson, C.J.; Snow, B.; Wang, Y.; Erdélyi, R. Evidence of ubiquitous Alfvén pulses transporting energy from the photosphere to the upper chromosphere. *Nat. Commun.* **2019**, *10*, 3504. [CrossRef] [PubMed]
118. Van Doorsselaere, T.; Srivastava, A.K.; Antolin, P.; Magyar, N.; Vasheghani Farahani, S.; Tian, H.; Kolotkov, D.; Ofman, L.; Guo, M.; Arregui, I.; et al. Coronal Heating by MHD Waves. *Space Sci. Rev.* **2020**, *216*, 140. [CrossRef]
119. Taroyan, Y.; Erdélyi, R. Heating Diagnostics with MHD Waves. *Space Sci. Rev.* **2009**, *149*, 229–254. [CrossRef]
120. Cargill, P.; de Moortel, I. Solar physics: Waves galore. *Nature* **2011**, *475*, 463–464. [CrossRef]
121. Jess, D.B.; Morton, R.J.; Verth, G.; Fedun, V.; Grant, S.D.T.; Giagkiozis, I. Multiwavelength Studies of MHD Waves in the Solar Chromosphere. An Overview of Recent Results. *Space Sci. Rev.* **2015**, *190*, 103–161. [CrossRef]
122. Stangalini, M. Wave energy in the solar atmosphere. *Nat. Astron.* **2023**, *7*, 761–762. [CrossRef]
123. Berghmans, D.; Clette, F. Active region EUV transient brightenings—First Results by EIT of SOHO JOP80. *Sol. Phys.* **1999**, *186*, 207–229. [CrossRef]
124. Ofman, L.; Nakariakov, V.M.; DeForest, C.E. Slow Magnetosonic Waves in Coronal Plumes. *Astrophys. J.* **1999**, *514*, 441–447. [CrossRef]
125. Ofman, L.; Nakariakov, V.M.; Sehgal, N. Dissipation of Slow Magnetosonic Waves in Coronal Plumes. *Astrophys. J.* **2000**, *533*, 1071–1083. [CrossRef]
126. Joarder, P.S.; Roberts, B. The modes of oscillation of a prominence. I—The slab with longitudinal magnetic field. *Astron. Astrophys.* **1992**, *256*, 264–272.
127. Joarder, P.S.; Roberts, B. The modes of oscillation of a prominence. II—The slab with transverse magnetic field. *Astron. Astrophys.* **1992**, *261*, 625–632.
128. Joarder, P.S.; Roberts, B. The modes of oscillation of a prominence. III. The slab in a skewed magnetic field. *Astron. Astrophys.* **1993**, *277*, 225.
129. Arregui, I.; Ballester, J.L. Damping Mechanisms for Oscillations in Solar Prominences. *Space Sci. Rev.* **2011**, *158*, 169–204. [CrossRef]
130. Oliver, R. Prominence Seismology Using Small Amplitude Oscillations. *Space Sci. Rev.* **2009**, *149*, 175–197. [CrossRef]
131. Yuan, D.; Nakariakov, V.M.; Huang, Z.; Li, B.; Su, J.; Yan, Y.; Tan, B. Oscillations in a Sunspot with Light Bridges. *Astrophys. J.* **2014**, *792*, 41. [CrossRef]
132. Yang, S.; Zhang, J.; Jiang, F.; Xiang, Y. Oscillating Light Wall Above a Sunspot Light Bridge. *Astrophys. J. Lett.* **2015**, *804*, L27. [CrossRef]
133. Hou, Y.J.; Li, T.; Yang, S.H.; Zhang, J. Light walls around sunspots observed by the Interface Region Imaging Spectrograph. *Astron. Astrophys.* **2016**, *589*, L7. [CrossRef]

134. Yang, S.; Zhang, J.; Erdélyi, R. Enhancement of a Sunspot Light Wall with External Disturbances. *Astrophys. J. Lett.* **2016**, *833*, L18. [CrossRef]
135. Yuan, D.; Walsh, R.W. Abnormal oscillation modes in a waning light bridge. *Astron. Astrophys.* **2016**, *594*, A101. [CrossRef]
136. Bharti, L. Fine structure above a light bridge in the transition region and corona. *Mon. Not. Roy. Astron. Soc.* **2015**, *452*, L16–L20. [CrossRef]
137. Rouppe van der Voort, L.H.M.; Hansteen, V.H.; Carlsson, M.; Fossum, A.; Marthinussen, E.; van Noort, M.J.; Berger, T.E. Solar magnetic elements at 0.1 arcsec resolution. II. Dynamical evolution. *Astron. Astrophys.* **2005**, *435*, 327–337. [CrossRef]
138. Crockett, P.J.; Mathioudakis, M.; Jess, D.B.; Shelyag, S.; Keenan, F.P.; Christian, D.J. The Area Distribution of Solar Magnetic Bright Points. *Astrophys. J. Lett.* **2010**, *722*, L188–L193. [CrossRef]
139. Keys, P.H.; Mathioudakis, M.; Jess, D.B.; Shelyag, S.; Christian, D.J.; Keenan, F.P. Tracking magnetic bright point motions through the solar atmosphere. *Mon. Not. Roy. Astron. Soc.* **2013**, *428*, 3220–3226. [CrossRef]
140. Berger, T.E.; Schrijver, C.J.; Shine, R.A.; Tarbell, T.D.; Title, A.M.; Scharmer, G. New Observations of Subarcsecond Photospheric Bright Points. *Astrophys. J.* **1995**, *454*, 531. [CrossRef]
141. Briand, C.; Solanki, S.K. Velocity fields below the magnetic canopy of solar flux tubes: Evidence for high-speed downflows? *Astron. Astrophys.* **1998**, *330*, 1160–1168.
142. Socas-Navarro, H.; Martínez Pillet, V.; Lites, B.W. Magnetic Properties of the Solar Internetwork. *Astrophys. J.* **2004**, *611*, 1139–1148. [CrossRef]
143. Danilovic, S.; Schüssler, M.; Solanki, S.K. Magnetic field intensification: Comparison of 3D MHD simulations with Hinode/SP results. *Astron. Astrophys.* **2010**, *509*, A76. [CrossRef]
144. Michalke, A. On the inviscid instability of the hyperbolictangent velocity profile. *J. Fluid Mech.* **1964**, *19*, 543–556. [CrossRef]
145. Blumen, W. Shear layer instability of an inviscid compressible fluid. *J. Fluid Mech.* **1970**, *40*, 769–781. [CrossRef]
146. Ray, T.P. The Effects of a Simple Shear Layer on the Growth of Kelvin–Helmholtz Instabilities. *Mon. Not. Roy. Astron. Soc.* **1982**, *198*, 617. [CrossRef]
147. Wu, D.; Wang, D. The Kelvin–Helmholtz instability of a cylindrical flow with a shear layer. *Mon. Not. Roy. Astron. Soc.* **1991**, *250*, 760–768. [CrossRef]